ISSN 0915-633X

NATIONAL INSTITUTE FOR FUSION SCIENCE

Molecular Dynamics Simulations of Structural Formation of a Single Polymer Chain: Bond-orientational Order and Conformational Defects

S. Fujiwara and T. Sato

(Received - Jan. 18, 1997)

NIFS-483 Feb. 1997

RESEARCH REPORT
NIFS Series

NAGOYA, JAPAN

Molecular dynamics simulations of structural formation of a single polymer chain: Bond-orientational order and conformational defects

Susumu Fujiwara and Tetsuya Sato

Theory and Computer Simulation Center, National Institute for Fusion Science, Oroshi, Toki 509-52, Japan

Abstract

The structural formation of a single polymer chain with 500 CH_2 groups is studied by the molecular dynamics simulations. Our simulations show that the bond-orientationally ordered structure at low temperatures is formed from a random-coil structure at high temperatures by a gradual stepwise cooling. From the radii of gyration and the bond-orientational order parameters, it is found that the anisotropy of a polymer chain also grows during the growth of the bond-orientational order. In the bond-orientationally ordered structure at low temperatures, 16 stems form a structure with deformed hexagonal symmetry and the stems in the outer layer have a tilted configuration. Furthermore, the *gauche* states are localized in the fold surface and the conformational states in the fold surface change more readily than those in the orientationally-ordered region.

Keywords: molecular dynamics simulation, polymer chain, structural formation, bond-orientational order, conformational defect

I. INTRODUCTION

Computer simulation of the structural formation of polymer chain systems has recently become the focus of attention in physics, chemistry and material science. Intensive studies of various model polymer systems, such as n-alkanes [1–8] and polyethylene chains [9–15], have been made in order to understand the dynamics of the ordered or partially ordered polymer chain systems.

Polymer chains show diverse static and dynamical structures since they have many internal degrees of freedom, for example the rotational freedom about each C-C bond in the polyethylene molecule. Owing to their structural diversity, polymeric materials have various mechanical and thermodynamical properties. It is well known that solution-grown single crystals of polyethylene are usually very thin lamellae whose width and thickness are respectively several tens of μm and $10 - 20$ nm, and consist of folded chains. Polyethylene chains are perpendicular to the fold surface [18–20]. Macroscopic properties of polyethylene single crystals have been studied by various experimental techniques: the molecular weight and the radius of gyration of the polymer chain can be obtained by the neutron scattering experiment and the lamellar thickness can be estimated by small angle x-ray scattering, electron spectroscopy and Raman scattering [20]. On the other hand, it seems very difficult to observe the structural formation process of polymer chains, such as the crystal growth process, *at the molecular level* by the present experimental techniques. Computer simulation is one of the strongest tools for investigating the mechanisms of the structural formation at the molecular level.

Over the last decade, several studies have been done in relation to the structural formation of polymer chain systems. Esselink *et al.* carried out molecular dynamics (MD) simulations of nucleation and melting of n-alkanes in order to determine the crystallization and melting temperatures and compute the crystallization rate of a nucleus [5]. Yamamoto *et al.* performed Monte Carlo (MC) simulations of the structure and the molecular mobility at free surfaces and the crystal/melt interfaces of an n-alkane crystal on the basis of the

rigid-chain assumption [6,7]. They also studied the dynamics of the conformational defects by MD simulations of a polyethylene chain confined in cylindrical potentials [13]. Noid *et al.* performed MD simulations on the motion of the conformational defects in a polyethylene-like crystal [9–12]. Kavassalis *et al.* carried out MD simulations of the folding process of a polyethylene chain below the equilibrium melting temperature [14,15]. Hikosaka *et al.* pointed out several important aspects of polymer crystallization: the existence of and the role played by a *metastable phase* and the high chain mobility associated with this phase [16,17].

The purpose of this paper is to clarify the mechanisms of the structural formation of polymer chains at the molecular level. In particular, our concern is to investigate the bond-orientational order and the conformational defects of polymer chains. With a view to investigating the process of the structural formation of polymer chains, we carry out the MD simulations of a single polymer chain and analyze the formation process of the orientationally ordered structure during cooling. Only few studies have so far been made at the transition process from the random-coil structure to the bond-orientationally ordered structure. Although Kavassalis *et al.* performed MD simulations of the structural formation of a polyethylene chain with the initial rotational isomeric state distribution, the bond-orientational order and the conformational defects were not analyzed [14].

In this study the effect of the interchain interaction is neglected. In order to take the effect of the interchain interaction into account, the MD simulations of many polymer chains will be carried out in the near future.

This paper is organized as follows. In Sec. II we describe in detail our simulation model and method. Our results obtained by MD simulations are presented in Sec. III. In Sec. IV summary and discussion are given.

II. MODEL AND METHOD

Following Ref. [14,15], the model polyethylene consists of a linear chain of n CH_2 groups, which are treated as united atoms (Fig. 1). The mass m of each CH_2 group is 14 g/mol. The united atoms interact via the bonded potentials (bond-stretching, bond-bending and torsional potentials) and the non-bonded potential. The atomic force field used here is the DREIDING potential [21]. The total potential energy $E_{\rm tot}$ consists of four parts: (i) the bond-stretching energies for C-C bonds,

$$E_{\rm stretch} = \sum_{i=2}^{n} \frac{1}{2} k_{\rm d} (d_i - d_0)^2, \tag{1}$$

where d_0 is the equilibrium bond length and d_i is the bond length between atoms $i-1$ and i, (ii) the bond-bending energies,

$$E_{\rm bend} = \sum_{i=3}^{n} \frac{1}{2} k_\theta (\theta_i - \theta_0)^2, \tag{2}$$

where θ_0 is the equilibrium bond angle and θ_i is the bond angle between three adjacent atoms $i-2$, $i-1$ and i, (iii) the torsional energies,

$$E_{\rm torsion} = \sum_{i=4}^{n} \frac{1}{2} v_\phi \left\{1 - \cos(3\phi_i)\right\}, \tag{3}$$

where ϕ_i is the dihedral angle formed by four consecutive atoms $i-3$, $i-2$, $i-1$ and i, and (iv) the 12-6 Lennard-Jones potential between non-bonded atoms separated by more than two bonds,

$$E_{\rm LJ} = \sum_{\substack{i=1 \\ (j-i\geq 3)}}^{n} \sum_{j=1}^{n} 4\epsilon \left[\left(\frac{\sigma}{r_{ij}} \right)^{12} - \left(\frac{\sigma}{r_{ij}} \right)^{6} \right], \tag{4}$$

where r_{ij} is the distance between atoms i and j. The values of all the potential parameters are listed in Table I.

The equations of motion for all atoms are solved numerically using the velocity version of the Verlet algorithm [22]. We apply the Nosé-Hoover method in order to keep the temperature of the system constant [23–25]. The integration time step is 0.001 ps and a relaxation

constant for the heat bath variable is 0.1 ps. The cutoff distance for the Lennard-Jones potential is 10.5 Å. The total momentum and the total angular momentum are taken to be zero in order to cancel overall translation and rotation of the chain.

The MD simulations are performed by the following procedure. First, a polymer chain with $n = 500$ united atoms is placed in the *all-trans* conformation with no total momentum and no total angular momentum. Secondly, we obtain random configuration of the polymer chain at high temperature ($T = 800$ K) by the MD run of 1000 ps. Thirdly, it is cooled stepwise to $T = 100$ K with the rate of 50 K/1000 ps (Fig. 2). Note that the equilibrium melting temperature of polyethylene is $T_{\mathrm{m}}^{\circ} = 414$ K, for reference.

In the following section, we study the bond-orientational order and the distribution of the dihedral angles at various temperatures in detail.

III. RESULTS

A. Chain conformations

In order to see the formation process of the orientationally ordered structure, we show, in Fig. 3, the snapshots of the chain conformation at time $t = 1000$ ps for various temperatures ($T = 800$, 500, 400 and 100 K) obtained by our MD simulations. In this figure, the ellipsoids, whose axes are determined as three principal axes of inertia, are depicted to roughly show the shape of a polymer chain. From Fig. 3(a), it is found that, at high temperature ($T = 800$ K), *gauche* states (deep green to light blue) are excited everywhere and a polymer chain forms a *random-coil structure.* Figures 3(b)-3(d) indicate that the orientationally ordered structure is formed at low temperatures by a stepwise cooling. It is also found that the chain configuration becomes more anisotropic as the temperature decreases. From Figs. 3(c) and 3(d), we find the following features concerning the obtained orientationally ordered structure: (i) the *gauche* excitations are located only in the fold surfaces, (ii) most bonds in the adjacently reentered fold are in the *gauche* state and (iii) in the non-adjacently reentered

fold, there are several *trans* bonds as well as *gauche* bonds.

In the following subsections, we analyze the radius of gyration, the bond-orientational order and the conformational defects in the process of the structural formation.

B. Radius of gyration

In Sec. III A, it was shown that the orientationally ordered structure at low temperatures is anisotropic. Here we introduce the coordinate system with three principal axes of inertia in order to analyze the anisotropic structure (Fig. 4). In this coordinate system, the origin is located at the center-of-mass position, the x-axis is the principal axis with the largest moment of inertia and the z-axis is that with the smallest moment of inertia. In this subsection, we investigate a change in the chain dimensions in the structural formation process.

The chain dimensions can be characterized by its radii of gyration parallel to individual axes defined as

$$R_{gx}^2 = \frac{1}{n}\sum_{i=1}^{n}\langle (x_i - x_c)^2 \rangle, \tag{5a}$$

$$R_{gy}^2 = \frac{1}{n}\sum_{i=1}^{n}\langle (y_i - y_c)^2 \rangle, \tag{5b}$$

$$R_{gz}^2 = \frac{1}{n}\sum_{i=1}^{n}\langle (z_i - z_c)^2 \rangle, \tag{5c}$$

where $\mathbf{r}_i = (x_i, y_i, z_i)$ is the position vector of the i-th atom, $\mathbf{r}_c = (x_c, y_c, z_c)$ is the position vector of the center of mass and $\langle \cdots \rangle$ denotes the ensemble average. The usual radius of gyration R_g is defined by

$$R_g^2 = \frac{1}{n}\sum_{i=1}^{n}\langle (\mathbf{r}_i - \mathbf{r}_c)^2 \rangle, \tag{6}$$

and the relation $R_g^2 = R_{gx}^2 + R_{gy}^2 + R_{gz}^2$ holds.

In Fig. 5, we show the temperature dependence of the radii of gyration. The time average is taken between 0.2 and 1.0 ns for each temperature. From the temperature dependence of

R_g, we find the following features: (i) At high temperatures ($T > 550$ K), R_g decreases as the temperature decreases. This temperature dependence is one of the characteristic features of a random coil. (ii) On the other hand, in the temperature region below $T = 550$ K, R_g increases as the temperature decreases. As is clearly seen from the temperature dependence of R_{gx}, R_{gy} and R_{gz}, the reason for this temperature dependence is that the shape of the polymer chain becomes more anisotropic as the temperature is reduced. From Fig. 5, the ratio R_{gz}/R_{gx} is found to be $R_{gz}/R_{gx} \approx 1.5$ at $T = 800$ K while $R_{gz}/R_{gx} \approx 2.9$ at $T = 100$ K. It will be ascertained by investigating the orientational order parameter in Sec. III C that the orientationally ordered structure is formed in this very temperature region. (iii) When the temperature is lower than $T = 400$ K, R_g is almost constant and the global change of the chain conformation is not recognized.

The radii of gyration R_g are plotted in Fig. 6 as a function of time for various temperatures. At $T = 800$ K (Fig. 6(a)) and $T = 100$ K (Fig. 6(d)), R_g only fluctuates around a mean value and no remarkable change is observed. It is seen in Fig. 6(b) that, at $T = 500$ K, after a gradual increase in the first 0.3 ns, R_g decreases slowly and then returns to the initial value. At $T = 400$ K (Fig. 6(c)), R_g increases gradually up to 0.6 ns and increases sharply during 0.6 and 0.7 ns. It is expected that an abrupt structural change might occur in this time interval. After the sharp increase, R_g stays at a constant value of about 1.29 nm, which is nearly equal to the value of R_g at lower temperatures.

C. Bond-orientational order

In this subsection, we study the bond-orientational order of a polymer chain. To begin with, we calculate the *global* bond-orientational order parameter A, which is defined by

$$A = \frac{1}{n}\sum_{i=3}^{n}\left\langle \frac{3\cos^2\psi_i - 1}{2} \right\rangle, \tag{7}$$

where ψ_i is the angle between the sub-bond vector $\mathbf{b}_i$ and the z-axis, and $\mathbf{b}_i = (\mathbf{d}_i + \mathbf{d}_{i-1})/2 = (\mathbf{r}_i - \mathbf{r}_{i-2})/2$ is the vector formed by connecting centers of two adjacent bonds i and $i-1$. The

parameter A would take a value of 1.0, 0.0 or -0.5, respectively, for a polymer chain whose sub-bonds are perfectly parallel, random or perpendicular to the z-axis. The parameter A is one of the simplest measures of the global bond-orientational order of a polymer chain. The global bond-orientational order parameter A versus temperature T is plotted in Fig. 7. At high temperatures above $T = 550$ K, the parameter A takes a value near zero, which shows that there is no global bond-orientational order in this temperature region. At lower temperatures than $T = 550$ K, A increases as the temperature decreases, which indicates that the global bond-orientational order grows below $T = 550$ K. The growth rate of the bond-orientational order below $T = 400$ K is smaller than that above $T = 400$ K, that is, the orientationally-ordered structure is formed around $T = 400$ K. It is found that in the temperature region where the global bond-orientational order grows, the anisotropy of a polymer chain also grows (Fig. 5). This suggests that the formation of the global bond-orientational order is closely related to the growth of the anisotropy of a polymer chain in the case of structural formation of a single polymer chain. This situation can change in the case of many-chain systems because of the existence of the interchain interaction.

We show the time dependence of the global bond-orientational order parameter A for various temperatures in Fig. 8. At $T = 800$ K, the parameter A fluctuates around zero. When the temperature is $T = 500$ K, the parameter A fluctuates around a nearly-constant value of 0.45 up to $t = 0.4$ ns, drops sharply to 0.35 at $t = 0.4$ ns and stays almost constant afterwards. This time dependence of A indicates that a relatively ordered state up to $t = 0.4$ ns is unstable. It can be seen from Table II that the total potential energy $E_{\rm tot}$ averaged before $t = 0.4$ ns is smaller than that averaged after $t = 0.4$ ns, that is, the state before $t = 0.4$ ns is *energetically* more stable than that after $t = 0.4$ ns. Therefore, the instability of the relatively ordered state up to $t = 0.4$ ns may be attributed to the *conformational entropy* of a polymer chain. The fact that the conformational entropy after $t = 0.4$ ns is larger than that before $t = 0.4$ ns is suggested by the following rough discussion on the fraction of the *trans* states ($|\phi| < \pi/3$), $P_{\rm trans}$, of a polymer chain (Table II). From Table II, it is found that the fraction $P_{\rm trans}$ after $t = 0.4$ is smaller than that before $t = 0.4$ ns.

Roughly speaking, the decrease of the fraction of the *trans* states means the increase of the available states, which indicates the increase of the conformational entropy. At $T = 400$ K, A increases gradually with time. Although the radius of gyration R_g rises abruptly between $t = 0.6$ and $t = 0.7$ ns (Fig. 6), the abrupt change in A is not found. It is worth noting that the way of change in $E_{\rm stretch}$ is opposite to that in $E_{\rm LJ}$, that is, $E_{\rm stretch}$ increases while $E_{\rm LJ}$ decreases, and vice versa (Fig. 9(b)). From Fig. 9(b), it is found that $E_{\rm bend}$ is constant and $E_{\rm torsion}$ decreases gradually in the formation process of the orientationally-ordered structure. At $T = 100$ K, there is no change in the parameter A.

In order to investigate the *local* bond-orientational order, we next calculate the bond-orientational order parameter $S_{\rm B}(z)$ which is defined by

$$S_{\rm B}(z) = \left\langle \left\langle \frac{3\cos^2(\psi(z)) - 1}{2} \right\rangle_{\rm bond} \right\rangle, \tag{8}$$

where $\psi(z)$ is the angle between the sub-bond vector $\mathbf{b}$ in a slab $[z,\, z + dz]$ and the z-axis, and $\langle \cdots \rangle_{\rm bond}$ denotes the average over the sub-bonds in a slab between z and $z + dz$. The parameter $S_{\rm B}(z)$ would take a value of 1.0, 0.0 or -0.5, respectively, for sub-bonds in a slab $[z, z + dz]$ perfectly parallel, random or perpendicular to the z-axis. We set $dz = 0.5\sigma$ in our calculations of $S_{\rm B}(z)$.

We show the bond-orientational order parameter $S_{\rm B}(z)$ at $t = 0.2$, 0.4, 0.6, 0.8 and 1.0 ns for various temperatures in Fig. 10. This figure shows the following features: (i) At high temperature ($T = 800$ K, Fig. 10(a)), $S_{\rm B}(z)$ is almost zero independent of z, which indicates that a polymer chain forms a random-coil structure. (ii) In the case of $T = 500$ K (Fig. 10(b)), a relatively orientationally-ordered structure is found to appear at $t = 0.2$ ns. The structure, however, breaks down after $t = 0.4$ ns. We have already discussed the cause of this breakdown in the earlier part of this subsection. (iii) At $T = 400$ K (Fig. 10(c)), it is clear that the more orientationally-ordered structure is formed with the elapse of time. (iv) At $T = 100$ K (Fig. 10(d)), the orientationally ordered structure is formed and there is a flat part between $z = -0.9$ and $z = 1.2$ nm. The bond-orientational order parameter $S_{\rm B}(z)$ in this flat region reaches 0.9, which indicates that the sub-bonds in this region are almost

parallel to the z-axis.

Finally, we analyze the orientationally ordered structure of a polymer chain obtained by our MD simulations in detail. It is useful to introduce the concept of "*stem*" in order to characterize the orientationally ordered structure. We define a *stem* as a series of atoms whose z-coordinates are located in the region ($z^{\rm s}_{\rm min} < z < z^{\rm s}_{\rm max}$) where $S_{\rm B}(z)$ is larger than 0.9 (Fig. 11). A snapshot of stems at $t = 1.0$ ns for $T = 100$ K is displayed in Fig. 12. In this case, $z^{\rm s}_{\rm min}$ and $z^{\rm s}_{\rm max}$ are set to be $z^{\rm s}_{\rm min} = -0.7$ nm and $z^{\rm s}_{\rm max} = 1.1$ nm, respectively. As clearly seen in this figure, 16 stems, each of which contains 14 or 15 atoms, form a bond-orientationally ordered structure with deformed hexagonal symmetry. The mean distance between stems is 0.416 nm, which corresponds to the minimum of the Lennard-Jones potential $R_0 = 0.40677$ nm. The length of stems ($z^{\rm s}_{\rm max} - z^{\rm s}_{\rm min}$) is about 1.8 nm and the thickness of the fold surface along the z-axis is around 1.0 nm; accordingly, the lamellar thickness in our simulations is about 3.8 nm. This value is several times as small as that of the lamellar thickness of solution-grown single crystals of polyethylene (10 – 20 nm). We expect that the lamellar thickness becomes large when the interchain interaction is taken into account. This was suggested in Ref. [14] in the case of four-chain system. It is found in Fig. 12(b) that the stems in the outer layer of the folded structure have a tilted configuration. As indicated by numbers beside stems in Fig. 12(b), which denote the connection of stems along the chain, the number of folds with nonadjacent reentry is about three times as many as that with adjacent reentry. The ratio of the nonadjacently-reentered to the adjacently-reentered folds may depend on the initial configuration and the cooling history.

D. conformational defects

In the previous subsections, we studied the formation process of the bond-orientationally ordered structure. In this subsection, we investigate the conformational defects in the bond-orientationally ordered structure. In Fig. 13, we show the histogram of the dihedral angles $P(\phi)$ at $z = 0$, 1.0 and 1.5 nm at several times for $T = 800$, 500, 400 and 100 K. Note

that the position at $z = 1.5$ nm corresponds to the inside of the fold surface at $T = 100$ K (Fig. 10). In Fig. 13(a), it is found that, at $T = 800$ K, there is no marked change in the shape of the histogram for any z and the distribution of ϕ is broad. At temperatures $T = 500$, 400 and 100 K (Figs. 13(b)-13(d)), the shape of the histogram depends on z. At $z = 0$ nm, almost all the conformations are *trans* around $\phi = 0$, especially for $T = 400$ and 100 K. On the other hand, the *gauche* states ($|\phi| > \pi/3$) are excited at $z = 1.0$ and 1.5 nm for $T = 500$ and 400 K and at $z = 1.5$ nm for $T = 100$ K. It is clearly seen in this figure that, even at low temperature ($T = 100$ K), the distribution $P(\phi)$ changes its shape with time at $z = 1.5$ nm. This fact suggests that the conformational motion is easy to occur at the fold surface even at low temperatures.

We show the three-dimensional plot of the distribution $P(\phi)$ at $t = 1.0$ ns for several temperatures in Fig. 14 in order to illustrate the dependence of $P(\phi)$ on z clearly. At $T = 800$ K, the distribution $P(\phi)$ does not depend on z very much. At low temperatures, on the other hand, $P(\phi)$ depends on z and the *gauche* states are located only in the fold surface.

IV. SUMMARY AND DISCUSSION

In this article, we have studied the formation process of the bond-orientationally ordered structure of a single polymer chain with 500 CH_2 groups during the gradual stepwise cooling by MD simulations. The bond-orientational order starts to grow at $T = 550$ K and the orientationally-ordered structure is formed at $T = 400$ K. New results obtained in our simulations are as follows:

i) The bond-orientationally ordered structure was formed from a random-coil structure by a gradual stepwise cooling.

ii) The anisotropy as well as the bond-orientational order of a polymer chain grew below $T = 550$ K.

iii) In the formation process of the bond-orientationally ordered structure at $T = 400$ K, the way of change in the bond-stretching energy E_{stretch} was opposite to that in the Lennard-Jones energy E_{LJ}.

iv) In the bond-orientationally ordered structure obtained by our simulations at $T = 100$ K, there were 16 stems, each of which involved 14 or 15 atoms. These stems formed a structure with deformed hexagonal symmetry and the stems in the outer layer had a tilted configuration.

v) In the bond-orientationally ordered structure at low temperatures, the *gauche* states were located exclusively in the fold surface and the conformational motion was easy to occur at the fold surface.

The second result, ii), suggests that the formation of the global bond-orientational order is closely related to the growth of the anisotropy of a polymer chain. However, there seems to be a possibility that this result is peculiar to the case of a single polymer chain. The existence of the interchain interaction may change the situation, that is, one polymer chain can form a bond-orientationally ordered structure with another chain as well as itself without changing into an anisotropic configuration. This problem is to be solved in the near future by performing the MD simulations of many polymer chains.

The fourth observation, iv), can be interpreted by the following simple argument. The energy loss due to the tilt of stems in the outer layer is considered to be small since the outer layer is a free surface. Therefore, the entanglement in the fold surface can be alleviated by the tilt of stems in the outer layer with the minimal energy loss.

Here we comment on the effect of the length of a polymer chain on the structural formation. In our simulations, we treated a relatively short polymer chain with 500 CH_2 groups. Whether the global bond-orientationally ordered structure is formed from a random-coil structure within a simulation time (at most a few tens of nano seconds) or not may depend on the length of a polymer chain. In the case of a very long polymer chain, it is expected that the aggregate of locally-ordered regions, such as a fringed micelle, is formed.

In this study, we concentrated on the analyses of the bond-orientational order and the conformational defects. In order to understand the mechanisms of the formation process of the bond-orientationally ordered structure clearly, we need analyze the molecular mobility and the conformational motion in this formation process. We will report the results of these analyses in a subsequent paper. Moreover, we will carry out the MD simulations of a many-chain system in order to take the effect of the interchain interaction into account. Furthermore, we plan to investigate the manner in which polymer chains are incorporated into the crystal surface from the point of view of *self-organization.*

ACKNOWLEDGMENTS

We would like to thank Drs. H. Takamaru, A. Kageyama and T.-H. Watanabe and other members of our complexity simulation group in National Institute for Fusion Science (NIFS) for their fruitful discussions and comments. This work was partially supported by the Grants-in-Aid from the Ministry of Education, Science and Culture. This work was carried out by using the Advanced Computing System for Complexity Simulation (NEC SX-3/24R) at NIFS.

REFERENCES

[1] T. Yamamoto, J. Chem. Phys. **82**, 3790 (1985); **89**, 2356 (1988).

[2] J. P. Ryckaert and M. L. Klein, J. Chem. Phys. **85**, 1613 (1986).

[3] J. P. Ryckaert, M. L. Klein and I. R. McDonald, Phys. Rev. Lett. **58**, 698 (1987).

[4] J. P. Ryckaert, I. R. McDonald and M. L. Klein, Molecular Physics **67**, 957 (1989).

[5] K. Esselink, P. A. J. Hilbers and B. W. H. van Beest, J. Chem. Phys. **101**, 9033 (1990).

[6] T. Yamamoto, M. Hikosaka and N. Takahashi, Macromolecules **27**, 1466 (1994).

[7] T. Yamamoto, J. Chem. Soc. Faraday Trans. **91**, 2559 (1995).

[8] S. N. Kreitmeier, G. L. Liang, D. W. Noid and B. Wunderlich, J. Chem. Soc. Faraday Trans. **91**, 2601 (1995).

[9] D. W. Noid, B. G. Sumpter and B. Wunderlich, Macromolecules **23**, 664 (1990); **24**, 4148 (1991).

[10] B. G. Sumpter, D. W. Noid, B. Wunderlich and S. Z. D. Cheng, Macromolecules **23**, 4671 (1990).

[11] B. G. Sumpter, D. W. Noid and B. Wunderlich, J. Chem. Phys. **93**, 6875 (1990).

[12] B. G. Sumpter, D. W. Noid and B. Wunderlich, Macromolecules **25**, 7247 (1992).

[13] T. Yamamoto and Y. Kimikawa, J. Chem. Phys. **97**, 5163 (1992); **99**, 6126 (1993).

[14] T. A. Kavassalis and P. R. Sundararajan, Macromolecules **26**, 4144 (1993).

[15] P. R. Sundararajan and T. A. Kavassalis, J. Chem. Soc. Faraday Trans. **91**, 2541 (1995).

[16] M. Hikosaka, S. Rastogi, A. Keller and H. Kawabata, J. Macromol. Sci. Phys. **B31**, 87 (1992).

[17] A. Keller, M. Hikosaka, S. Rastogi, A. Toda, P. J. Barham and G. Goldbeck-Wood,

J. Mater. Sci. **29**, 2579 (1994).

[18] A. Keller, Rep. Prog. Phys. **31**, 623 (1968).

[19] B. Wunderlich, *Macromolecular Physics, Vol. 1, Crystal Structure, Morphology, Defects* (Academic, New York, 1976).

[20] P. J. Phillips, Rep. Prog. Phys. **53**, 549 (1990).

[21] S. L. Mayo, B. D. Olafson and W. A. Goddard III, J. Phys. Chem. **94**, 8897 (1990).

[22] L. Verlet, Phys. Rev. **159**, 98 (1967).

[23] S. Nosé, Mol. Phys. **52**, 255 (1984).

[24] S. Nosé, J. Chem. Phys. **81**, 511 (1984).

[25] W. G. Hoover, Phys. Rev. A **31**, 1695 (1985).

FIGURES

FIG. 1. A model polyethylene chain. Each CH_2 group is treated as a spherical united atom. The bond length d_i is calculated as $d_i = |\mathbf{d}_i|$, where $\mathbf{d}_i \equiv \mathbf{r}_i - \mathbf{r}_{i-1}$ is the bond vector between atoms $i-1$ and i, and $\mathbf{r}_i$ denotes the position vector of atom i. The bond angle θ_i is the angle between three adjacent atoms $i-2$, $i-1$ and i, and the dihedral angle ϕ_i is the angle between the plane formed by $\mathbf{d}_{i-2}$ and $\mathbf{d}_{i-1}$ and that formed by $\mathbf{d}_{i-1}$ and $\mathbf{d}_i$. The *trans* conformation corresponds to $\phi = 0$.

FIG. 2. Schematic explanation of the cooling process. The cooling rate is 50 K/ns.

FIG. 3. The chain conformation of a polyethylene chain at 1000 ps (a) for $T = 800$ K, (b) for $T = 500$ K, (c) for $T = 400$ K and (d) for $T = 100$ K (Left: side view, Right: top view). Color denotes the absolute value of the dihedral angle around each bond and the ellipsoid roughly shows the shape of a polyethylene chain. The end bonds are colored with blue.

FIG. 4. Explanation of the coordinate system with three principal axes of inertia. The origin of the coordinates is the center of mass. The main axis (z-axis) is determined as the principal axis with the smallest moment of inertia and the x-axis is the principal axis with the largest moment of inertia.

FIG. 5. The radii of gyration R_{gx}, R_{gy}, R_{gz}, R_g vs. temperature T. Time average is taken between 0.2 and 1.0 ns.

FIG. 6. The radius of gyration R_g vs. time t (a) at $T = 800$ K, (b) at $T = 500$ K, (c) at $T = 400$ K and (d) at $T = 100$ K.

FIG. 7. The global bond-orientational order parameter A vs. temperature T. Time average is taken between 0.2 and 1.0 ns.

FIG. 8. The global bond-orientational order parameter A vs. time t for (a) $T = 800$ K, (b) $T = 500$ K, (c) $T = 400$ K and (d) $T = 100$ K.

FIG. 9. The bond-stretching energy $E_{\rm stretch}$, the bond-bending energy $E_{\rm bend}$, the torsional energy $E_{\rm torsion}$ and the Lennard-Jones energy $E_{\rm LJ}$ vs. time t (a) at $T = 500$ K and (b) at $T = 400$ K.

FIG. 10. The bond-orientational order parameter $S_{\rm B}(z)$ vs. z at $t = 0.2$, 0.4, 0.6, 0.8 and 1.0 ns for (a) $T = 800$ K, (b) $T = 500$ K, (c) $T = 400$ K and (d) $T = 100$ K.

FIG. 11. Schematic explanation of stems. Each stem is defined as a series of atoms whose z-components are located between $z^{\rm s}_{\rm min}$ and $z^{\rm s}_{\rm max}$.

FIG. 12. The configuration of stems at $t = 1.0$ ns for $T = 100$ K; (a) side view and (b) top view. Numbers beside stems in (b) denote the connection of stems along the chain. Filled circles represent the central positions of individual stems.

FIG. 13. Distribution of the dihedral angle $P(\phi)$ at times $t = 0.2$, 0.4, 0.6, 0.8 and 1.0 ns at $z = 0$, 1.0 and 1.5 nm for (a) $T = 800$ K, (b) $T = 500$ K, (c) $T = 400$ K and (d) $T = 100$ K. In the low temperatures ($T = 400$ and 100 K), $z = 1.0$ nm corresponds to $z^{\rm s}_{\rm max}$ and the position at $z = 1.5$ nm is inside the fold surface.

FIG. 14. Three-dimensional plot of the distribution $P(\phi)$ as a function of ϕ and z at $t = 1.0$ ns for (a) $T = 800$ K, (b) $T = 500$ K, (c) $T = 400$ K and (d) $T = 100$ K.

TABLES

TABLE I. Potential energy parameters used in our simulation [21].

parameter	value	unit
d_0	0.153	nm
θ_0	1.2310	rad
k_d	70000	kcal/nm^2·mol
k_θ	100	kcal/rad^2·mol
k_ϕ	2.0	kcal/mol
ϵ	0.1984	kcal/mol
σ	0.36239	nm

TABLE II. Average potential energies and the fraction of the *trans* states ($|\phi| < \pi/3$) P_trans at $T = 500$ K before $t = 0.4$ ns and after $t = 0.4$ ns.

	average before $t = 0.4$ ns	average after $t = 0.4$ ns
E_stretch	255.9 ± 16.2 (kcal/mol)	243.6 ± 14.1 (kcal/mol)
E_bend	245.8 ± 15.3 (kcal/mol)	252.9 ± 16.1 (kcal/mol)
E_torsion	295.7 ± 14.3 (kcal/mol)	306.9 ± 13.4 (kcal/mol)
E_LJ	-754.5 ± 20.6 (kcal/mol)	-734.0 ± 19.8 (kcal/mol)
E_tot	42.9 ± 36.7 (kcal/mol)	69.4 ± 32.1 (kcal/mol)
P_trans	0.849 ± 0.016	0.832 ± 0.015

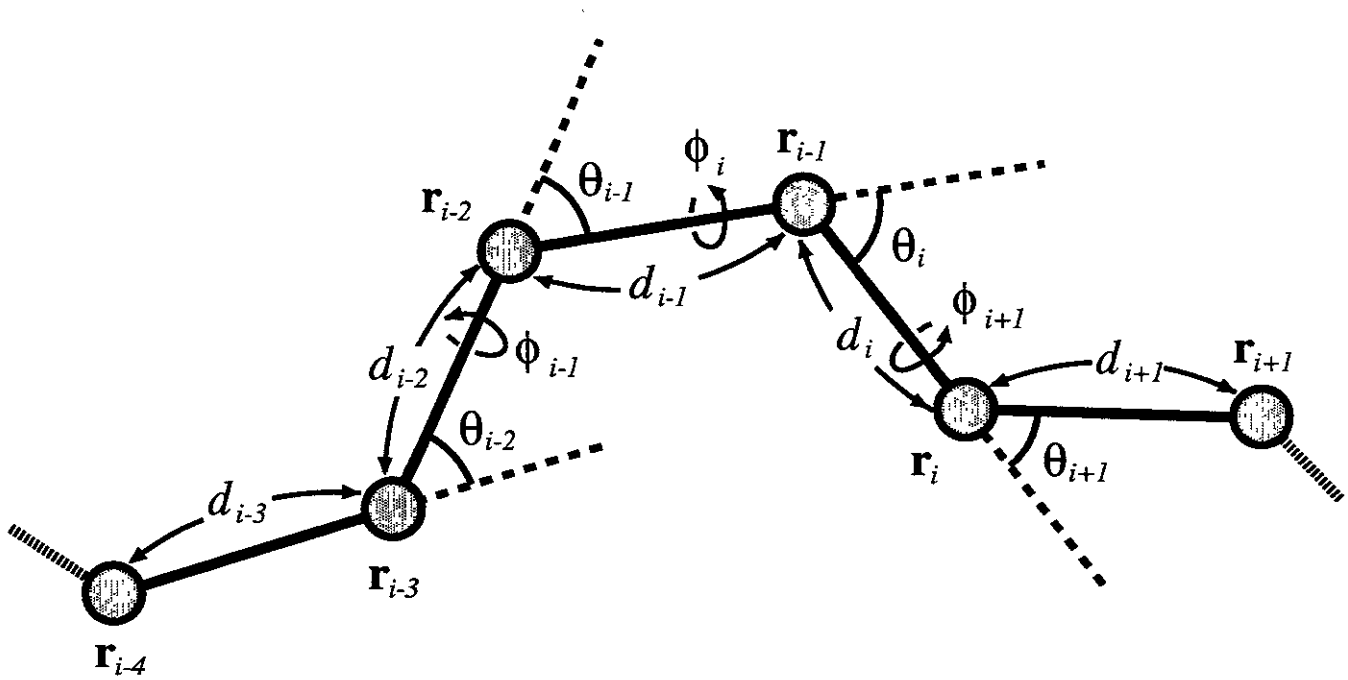
$\mathbf{r}_{i-4}$
$\mathbf{r}_{i-3}$
$\mathbf{r}_{i-2}$
$\mathbf{r}_{i-1}$
$\mathbf{r}_i$
$\mathbf{r}_{i+1}$
d_{i-3}
d_{i-2}
d_{i-1}
d_i
d_{i+1}
θ_{i-2}
θ_{i-1}
θ_i
θ_{i+1}
ϕ_{i-1}
ϕ_i
ϕ_{i+1}

Fig. 1

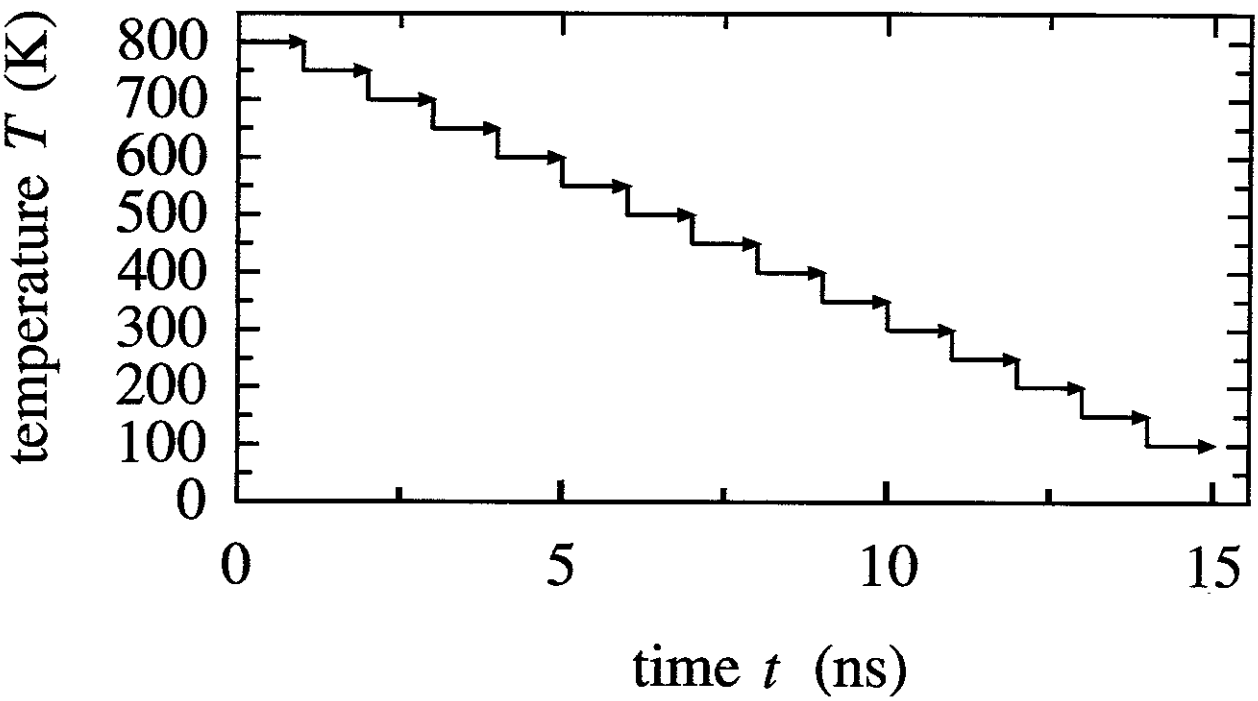
temperature T (K)
800
700
600
500
400
300
200
100
0
0
5
10
15
time t (ns)

Fig. 2

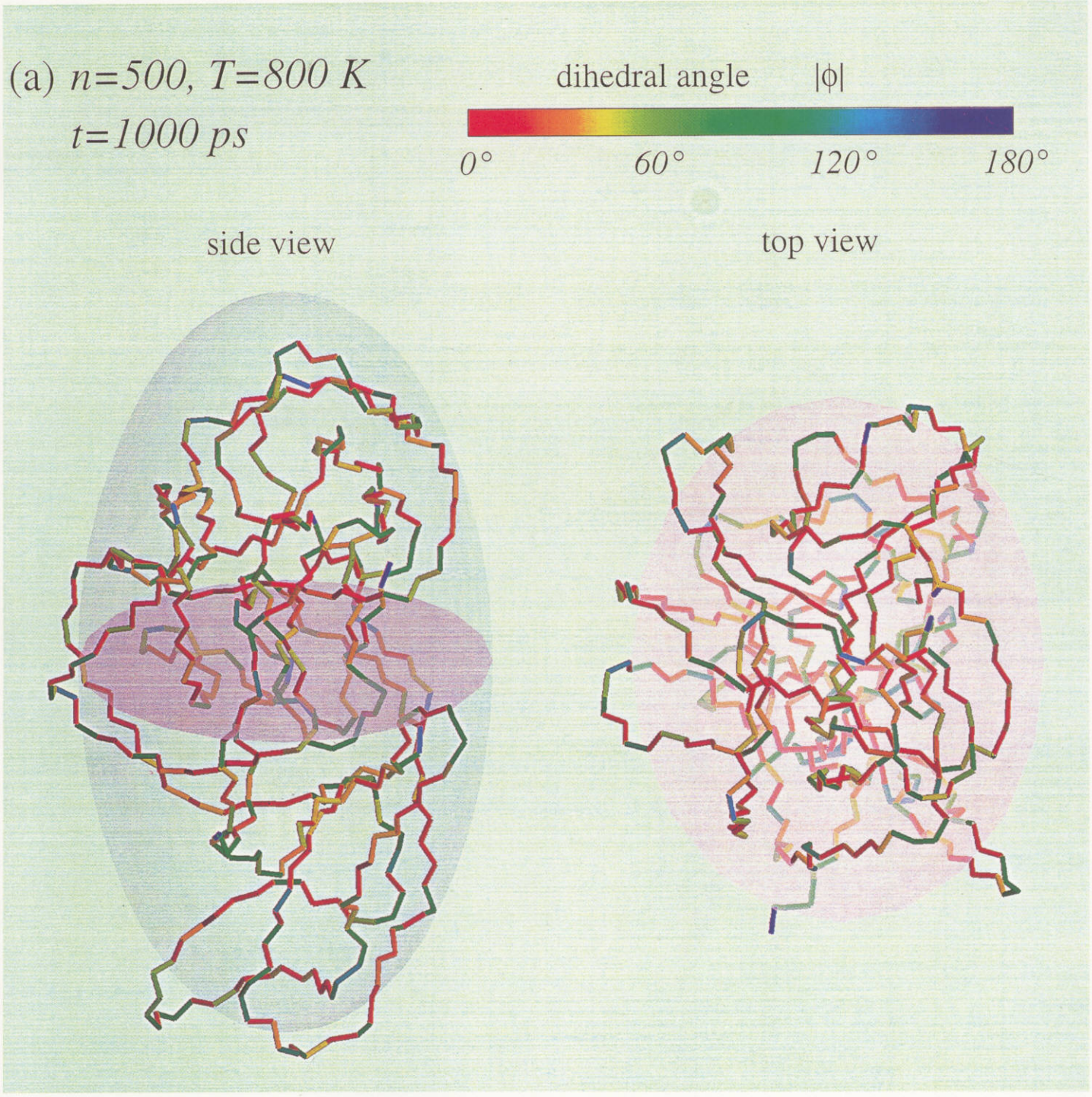
(a) n=500, T=800 K
t=1000 ps
dihedral angle |ϕ|
0°
60°
120°
180°
side view
top view

Fig. 3 (a)

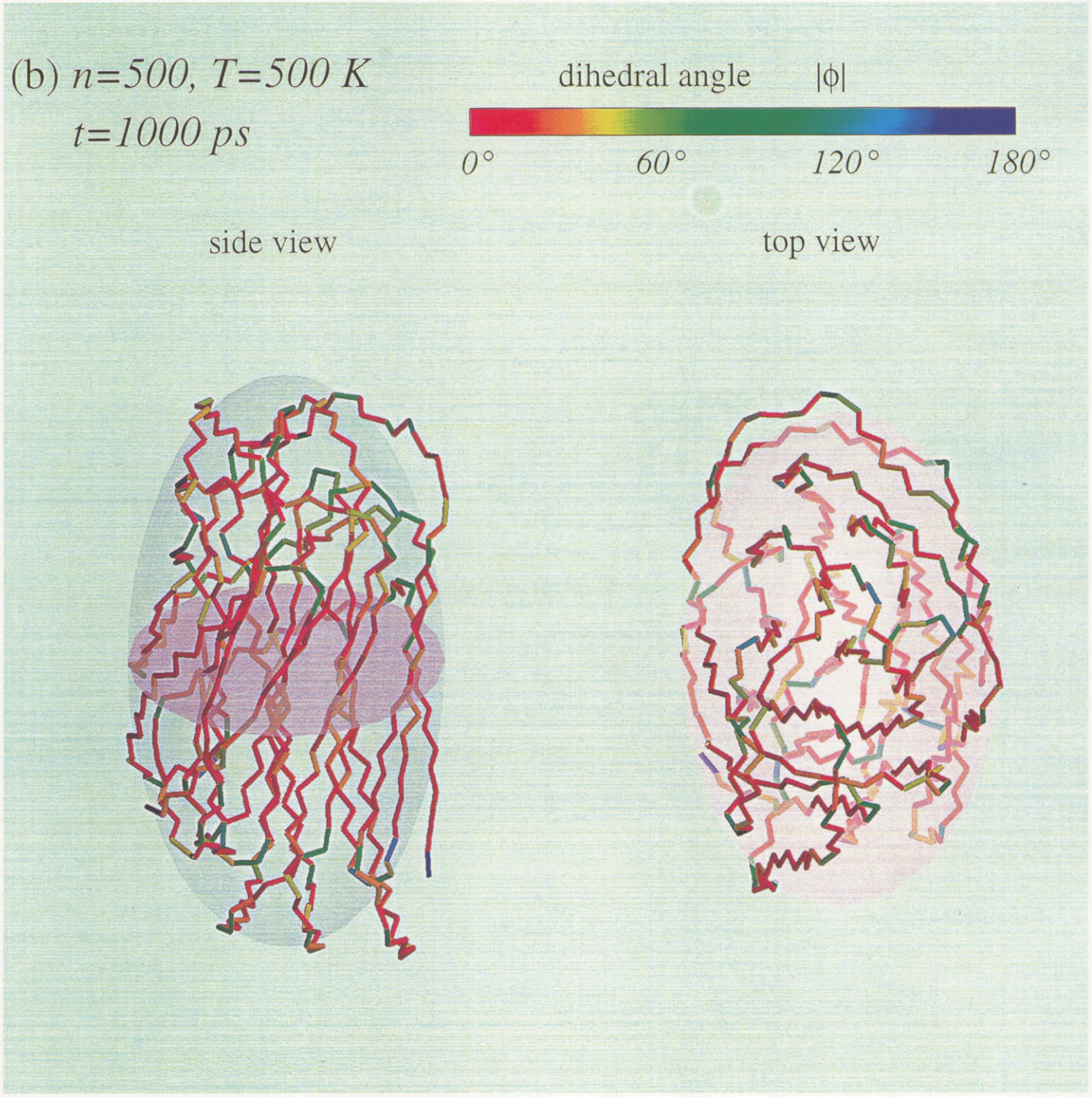
(b) n=500, T=500 K
t=1000 ps
dihedral angle |ϕ|
0°
60°
120°
180°
side view
top view

Fig. 3 (b)

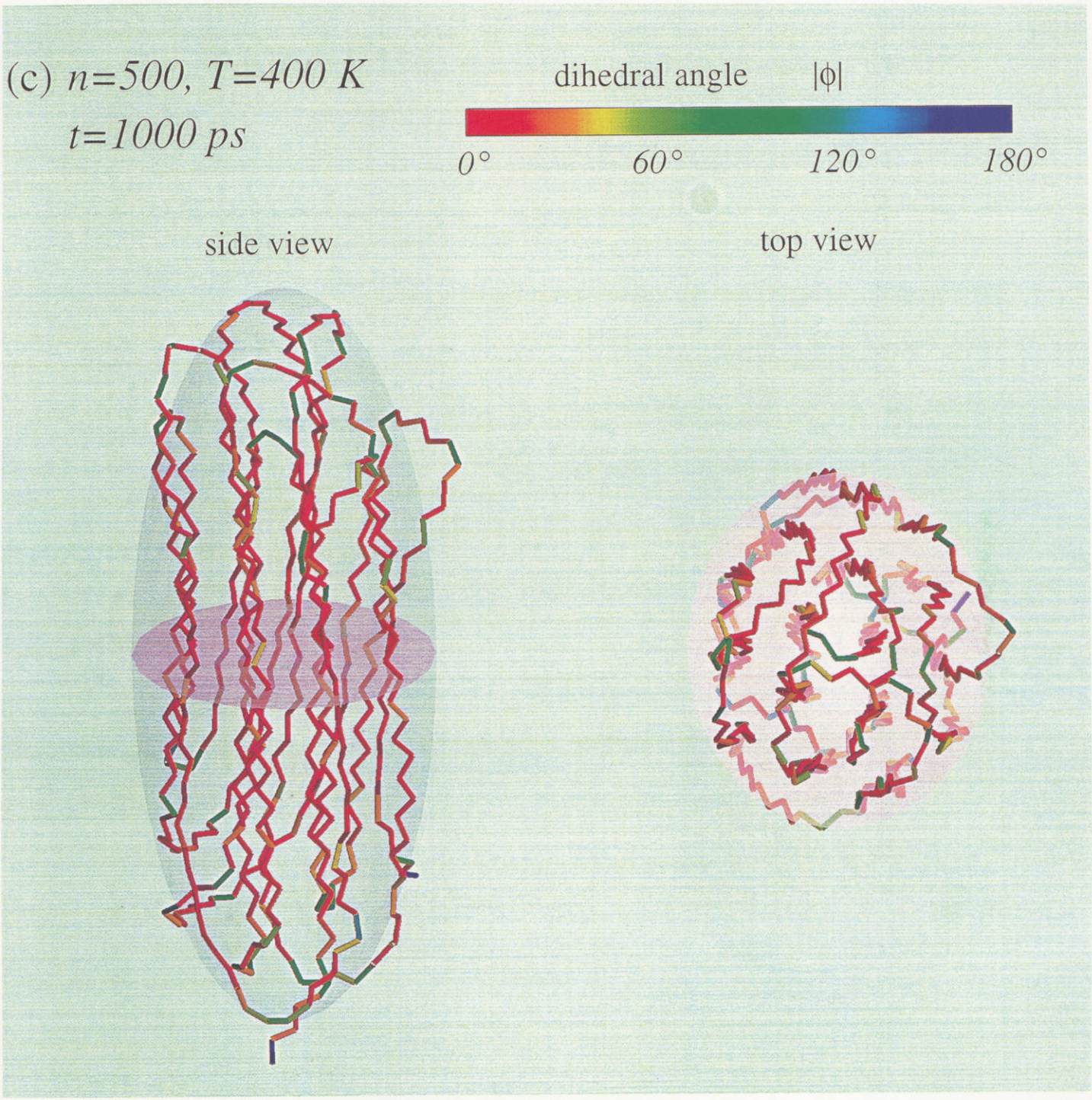
(c) n=500, T=400 K
t=1000 ps
dihedral angle |ϕ|
0°
60°
120°
180°
side view
top view

Fig. 3 (c)

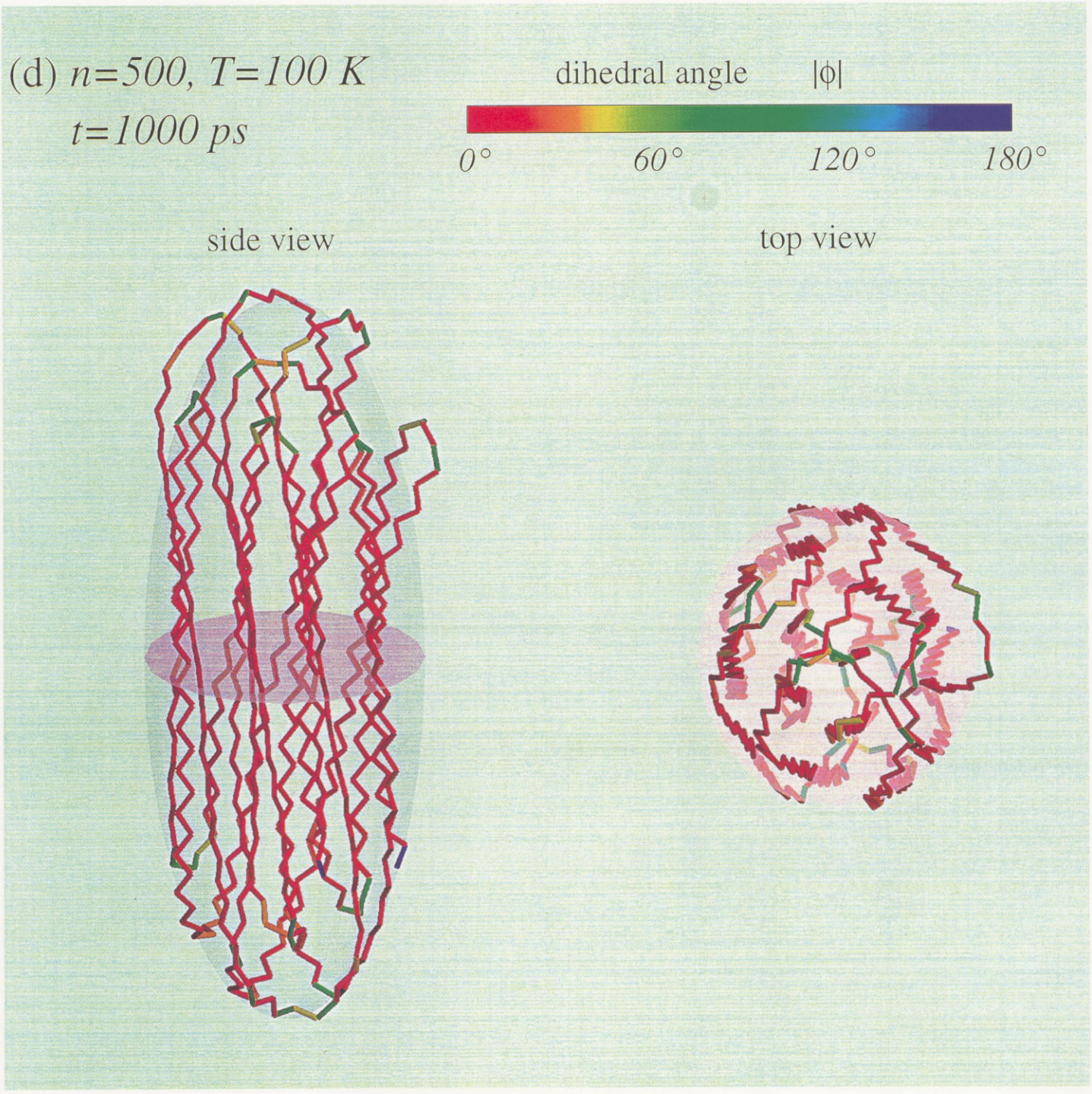
(d) n=500, T=100 K
t=1000 ps
dihedral angle |ϕ|
0°
60°
120°
180°
side view
top view

Fig. 3 (d)

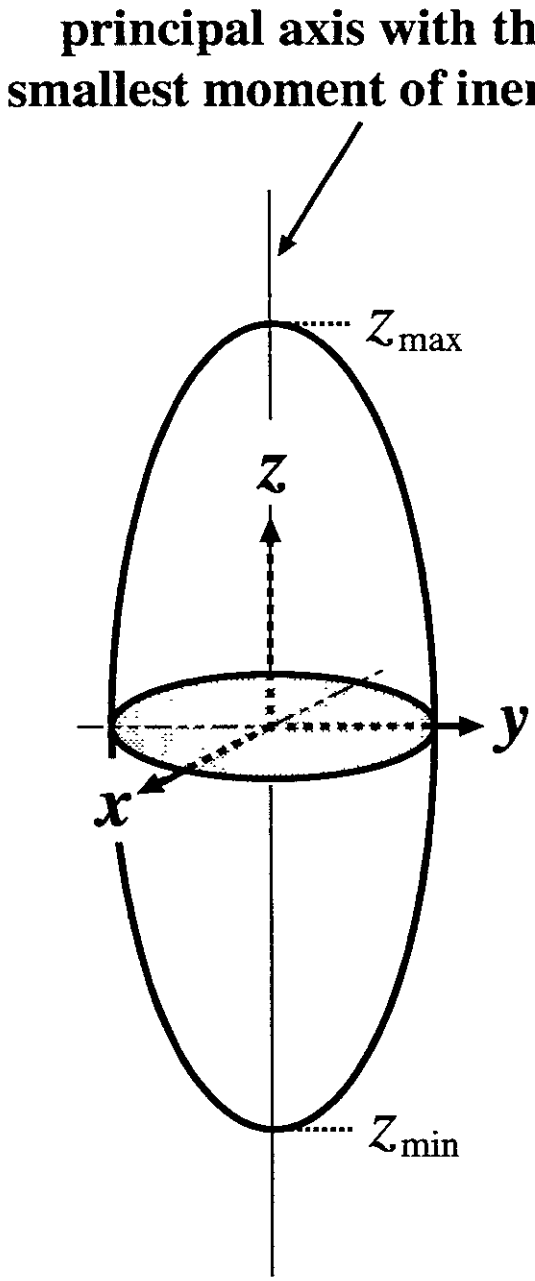
principal axis with the
smallest moment of inertia
z_{max}
z
y
x
z_{min}

Fig. 4

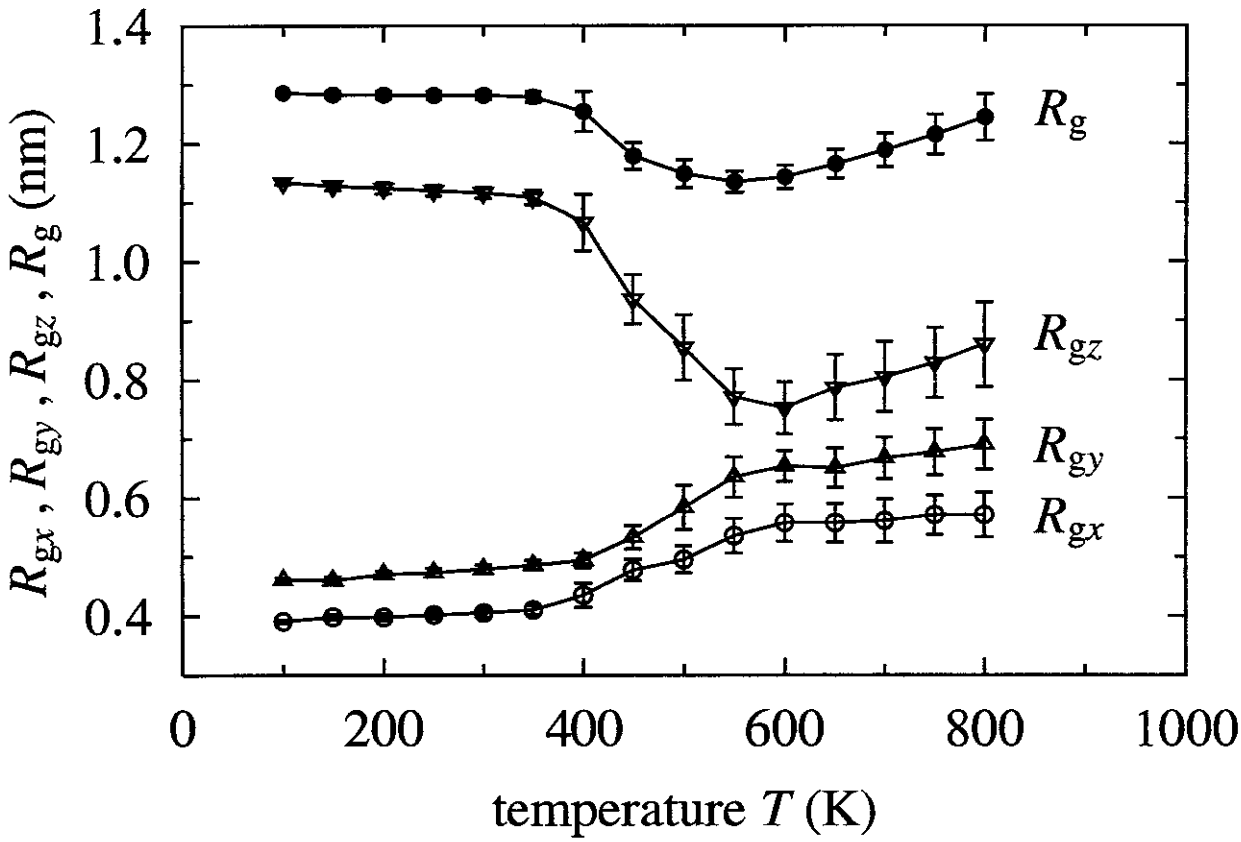
1.4
1.2
1.0
0.8
0.6
0.4
R_{gx} , R_{gy} , R_{gz} , R_g (nm)
R_g
R_{gz}
R_{gy}
R_{gx}
0
200
400
600
800
1000
temperature T (K)

Fig. 5

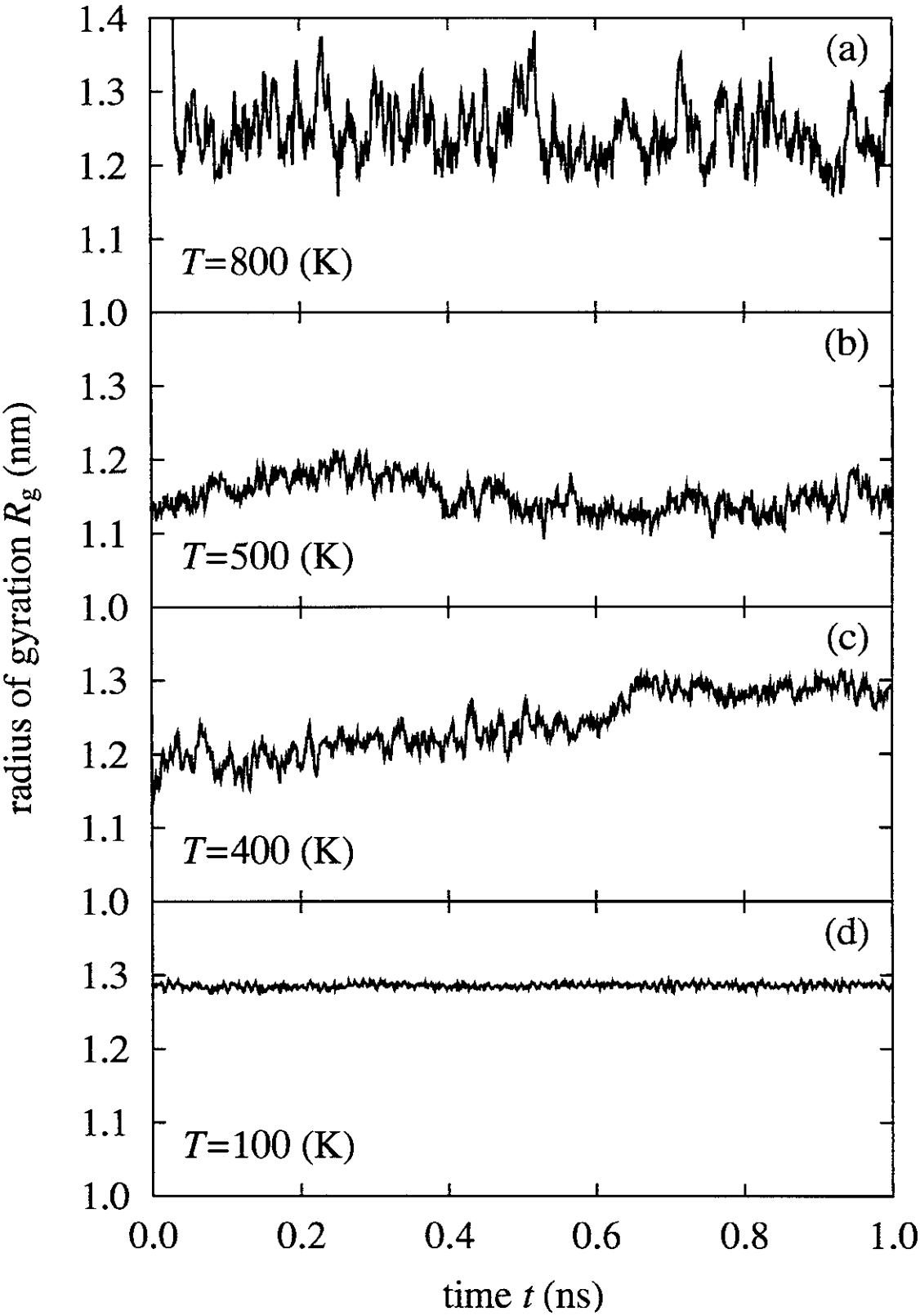
radius of gyration R_g (nm)
time t (ns)
(a)
T=800 (K)
(b)
T=500 (K)
(c)
T=400 (K)
(d)
T=100 (K)
1.4
1.3
1.2
1.1
1.0
0.0
0.2
0.4
0.6
0.8
1.0

Fig. 6

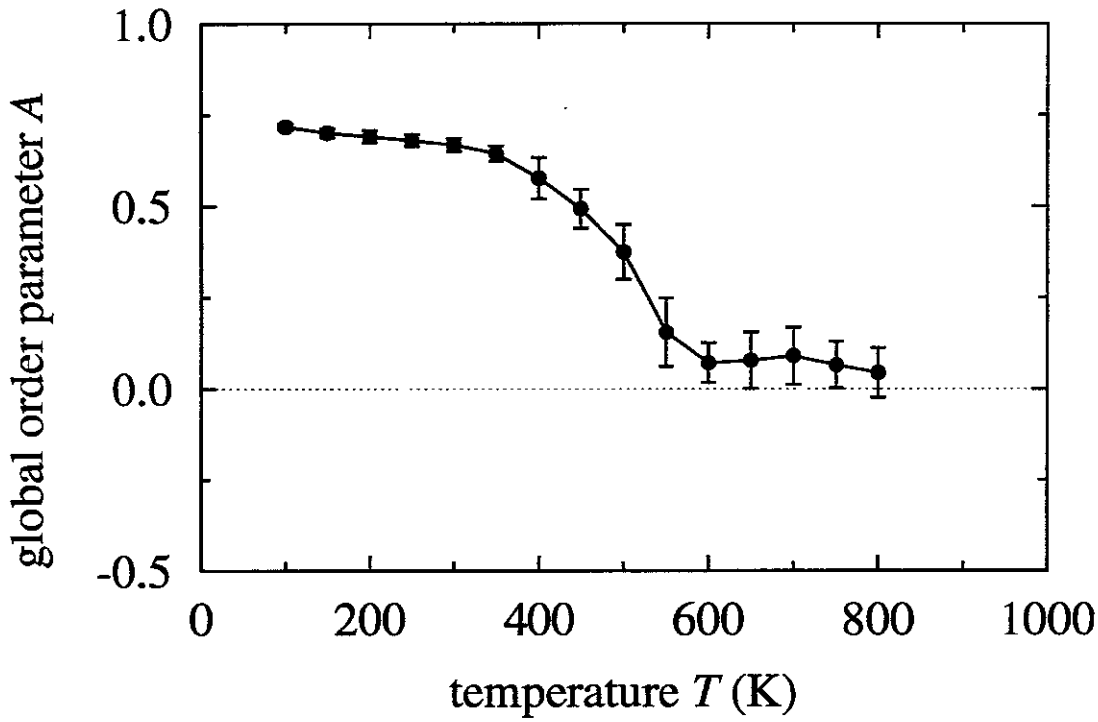
1.0
0.5
0.0
-0.5
0
200
400
600
800
1000
global order parameter A
temperature T (K)

Fig. 7

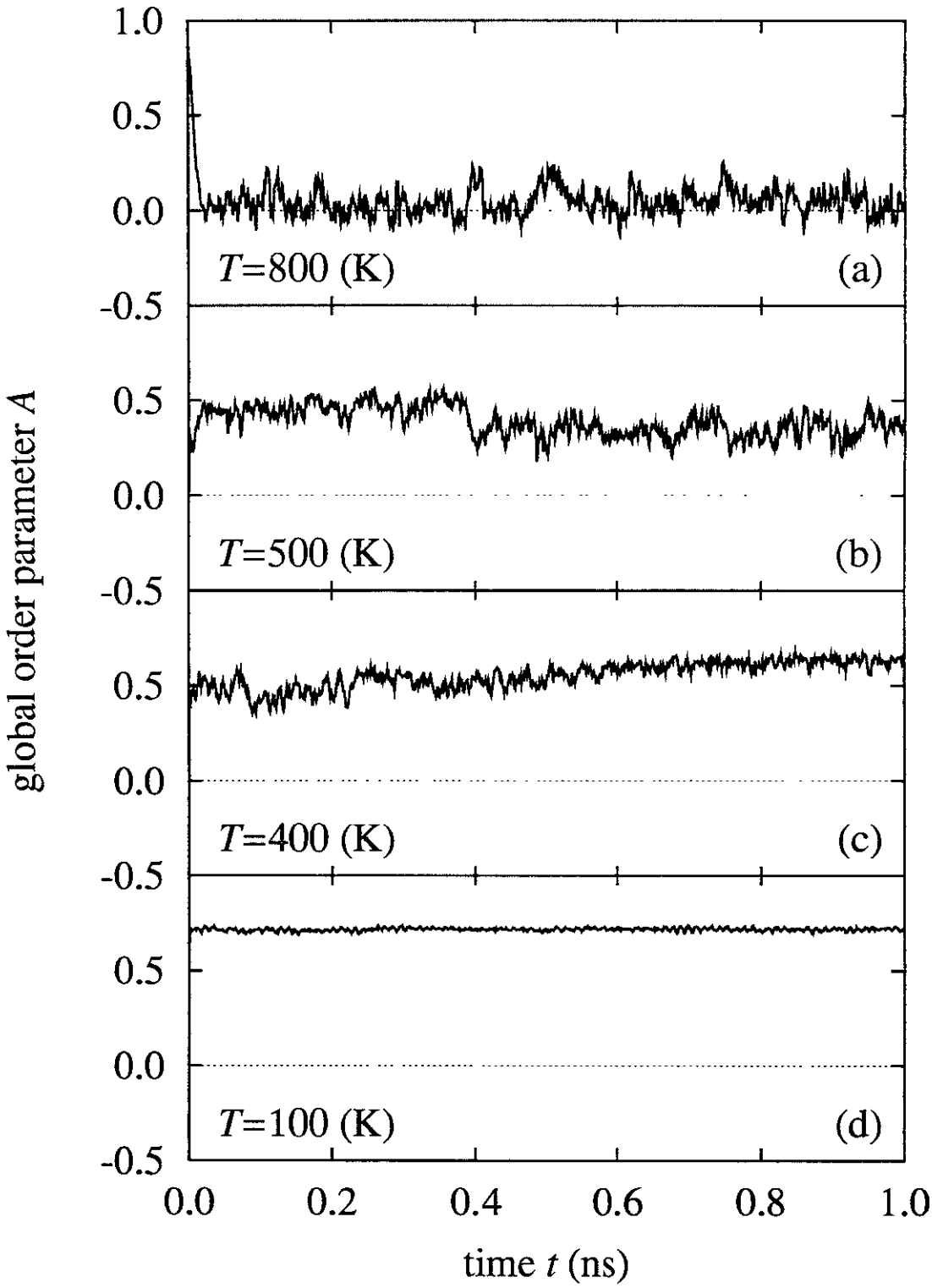
1.0
0.5
0.0
-0.5
T=800 (K)
(a)
0.5
0.0
-0.5
T=500 (K)
(b)
0.5
0.0
-0.5
T=400 (K)
(c)
0.5
0.0
-0.5
T=100 (K)
(d)
0.0
0.2
0.4
0.6
0.8
1.0
time t (ns)
global order parameter A

Fig. 8

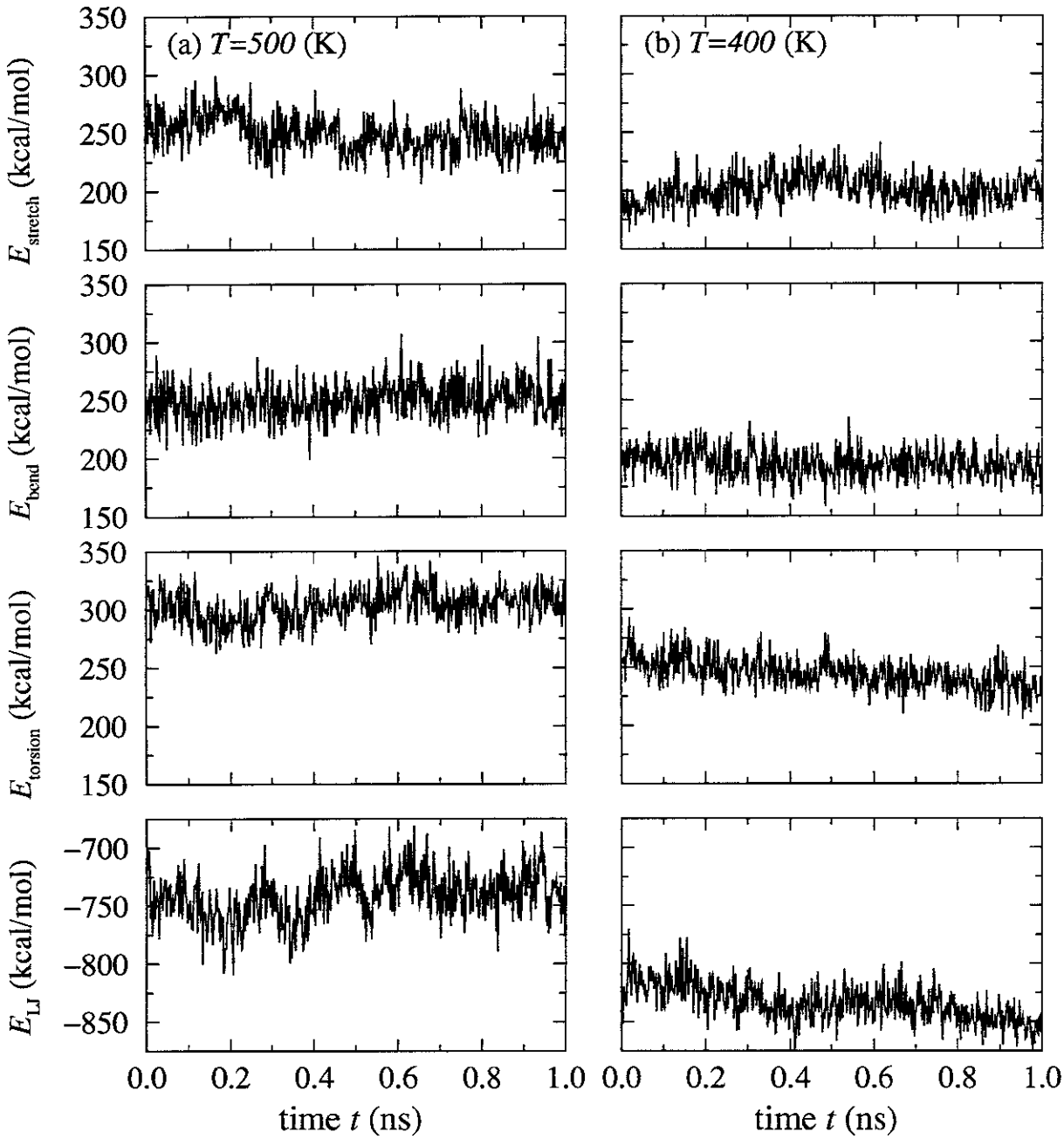
(a) T=500 (K)
(b) T=400 (K)
E_stretch (kcal/mol)
E_bend (kcal/mol)
E_torsion (kcal/mol)
E_LJ (kcal/mol)
350
300
250
200
150
−700
−750
−800
−850
0.0
0.2
0.4
0.6
0.8
1.0
time t (ns)

Fig. 9

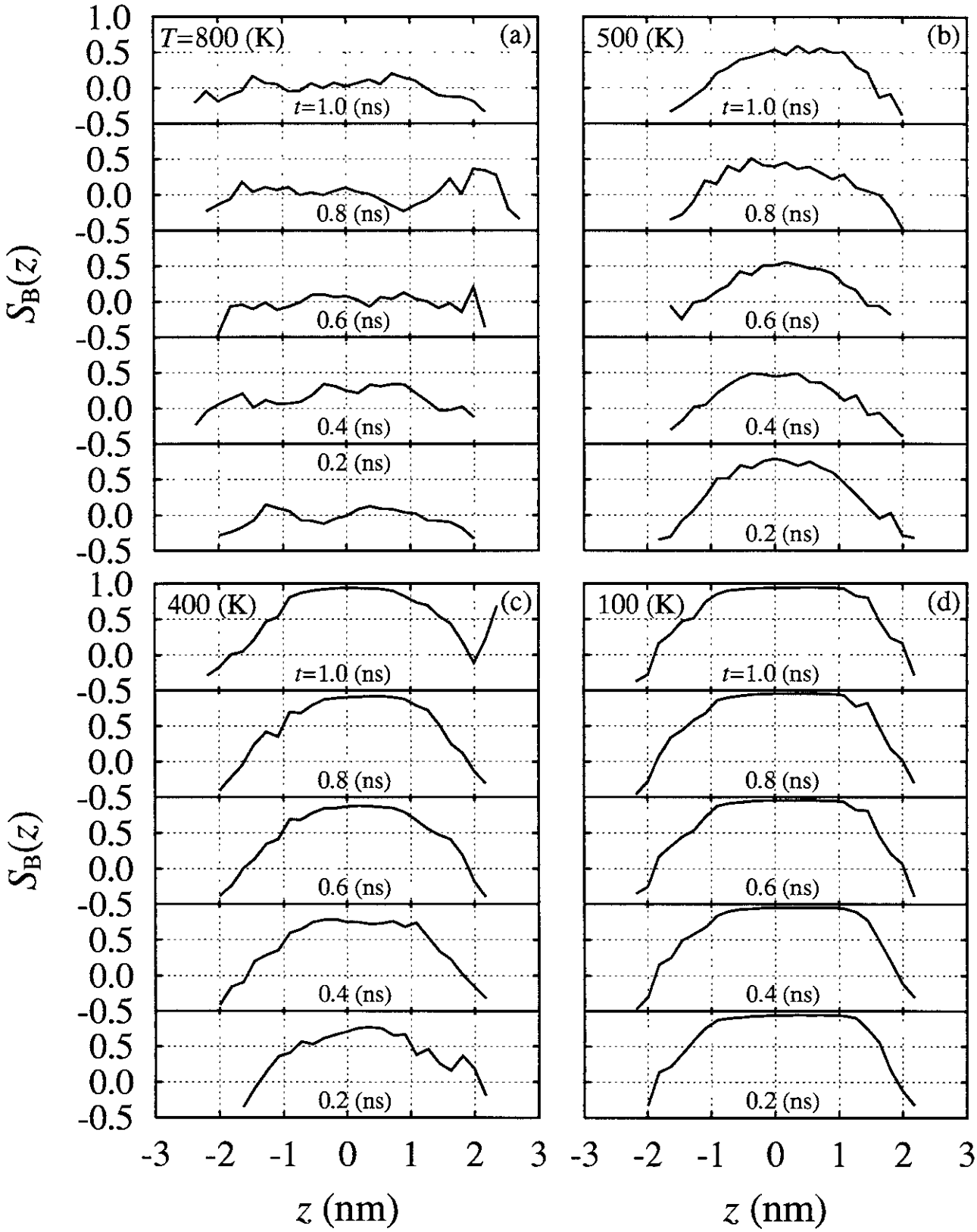

Fig. 10

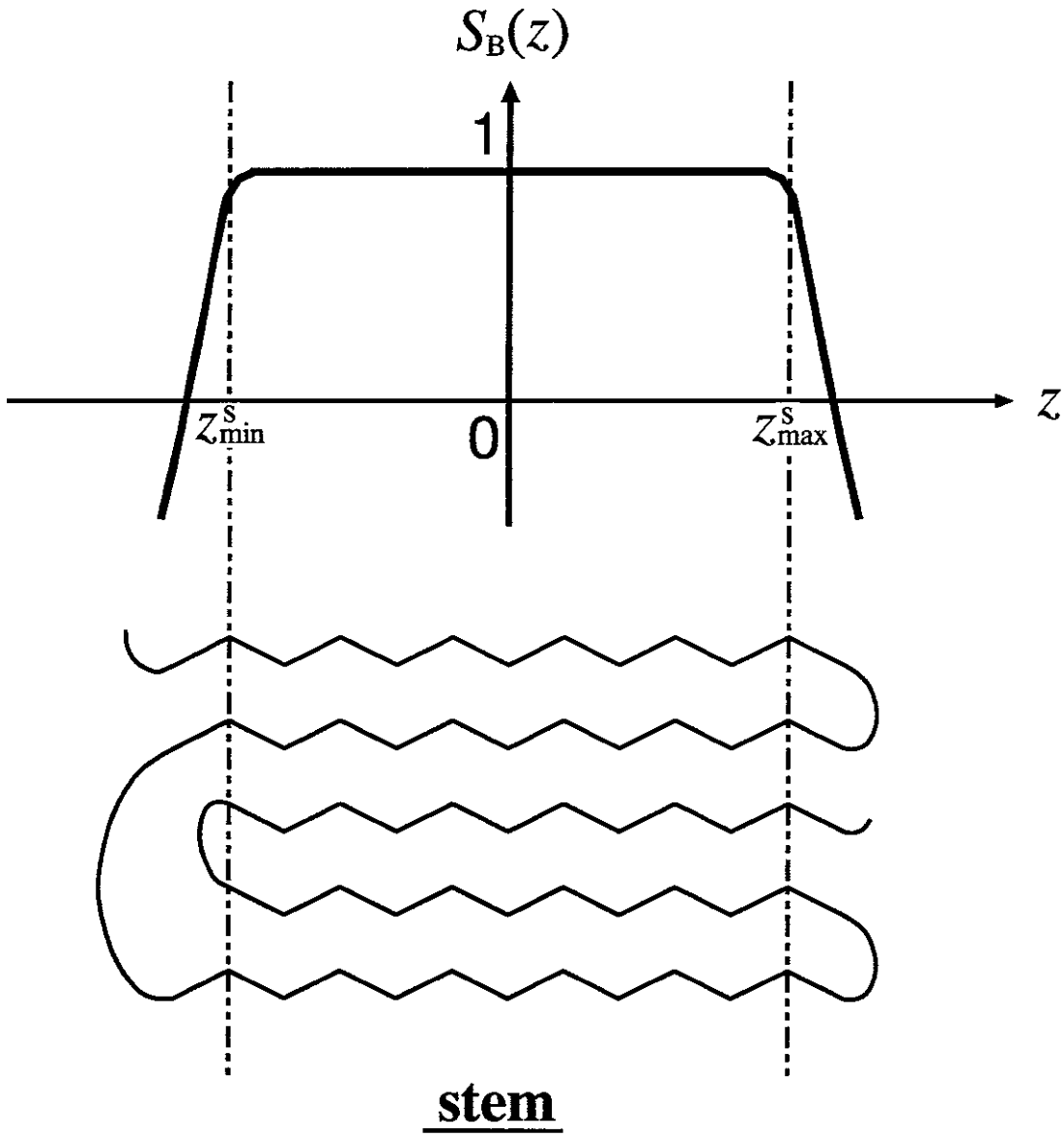

Fig. 11

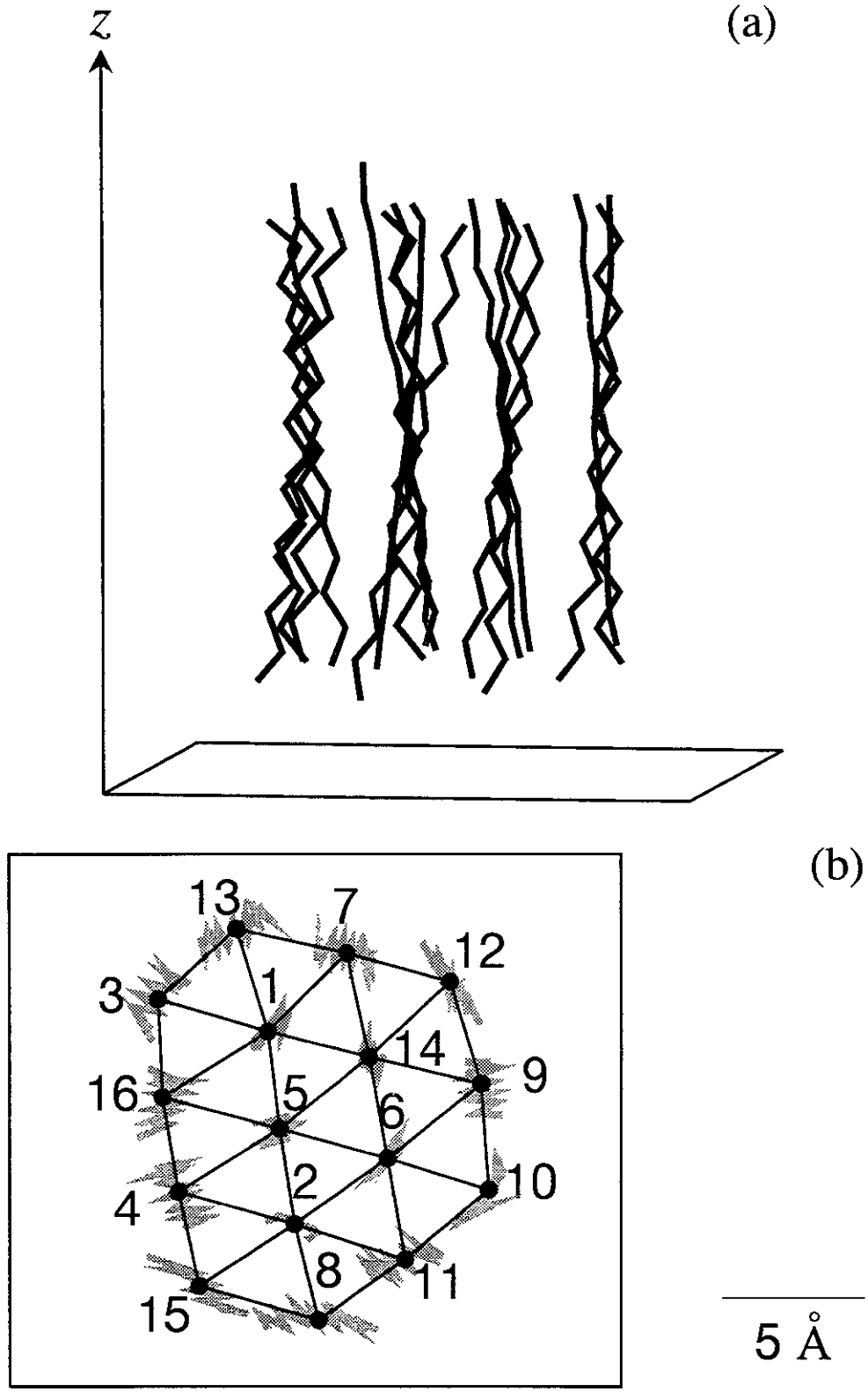

Fig. 12

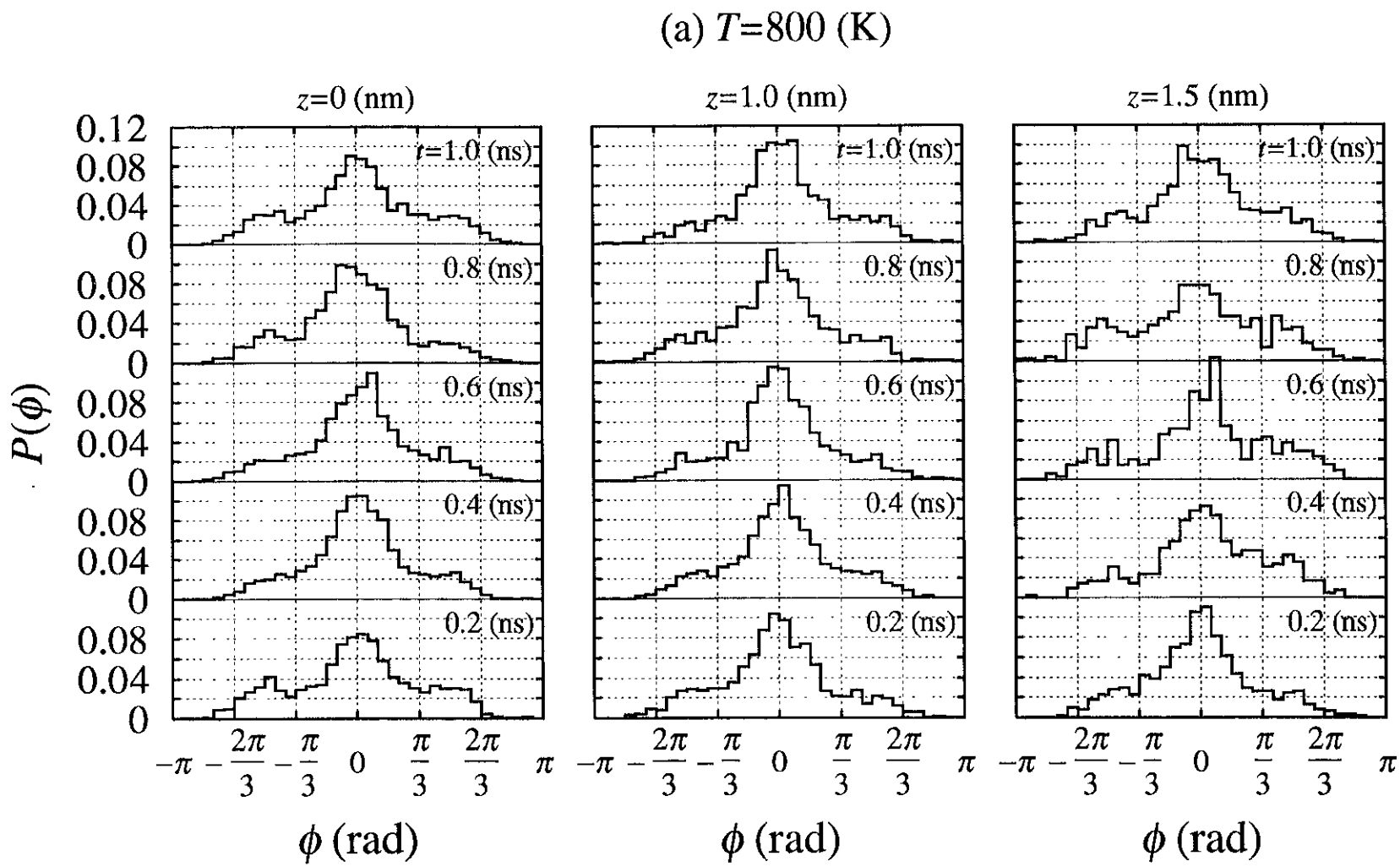
(a) T=800 (K)
z=0 (nm)
z=1.0 (nm)
z=1.5 (nm)
t=1.0 (ns)
0.8 (ns)
0.6 (ns)
0.4 (ns)
0.2 (ns)
$P(\phi)$
0.12
0.08
0.04
0
$-\pi$ $-\frac{2\pi}{3}$ $-\frac{\pi}{3}$ 0 $\frac{\pi}{3}$ $\frac{2\pi}{3}$ π
ϕ (rad)

Fig. 13(a)

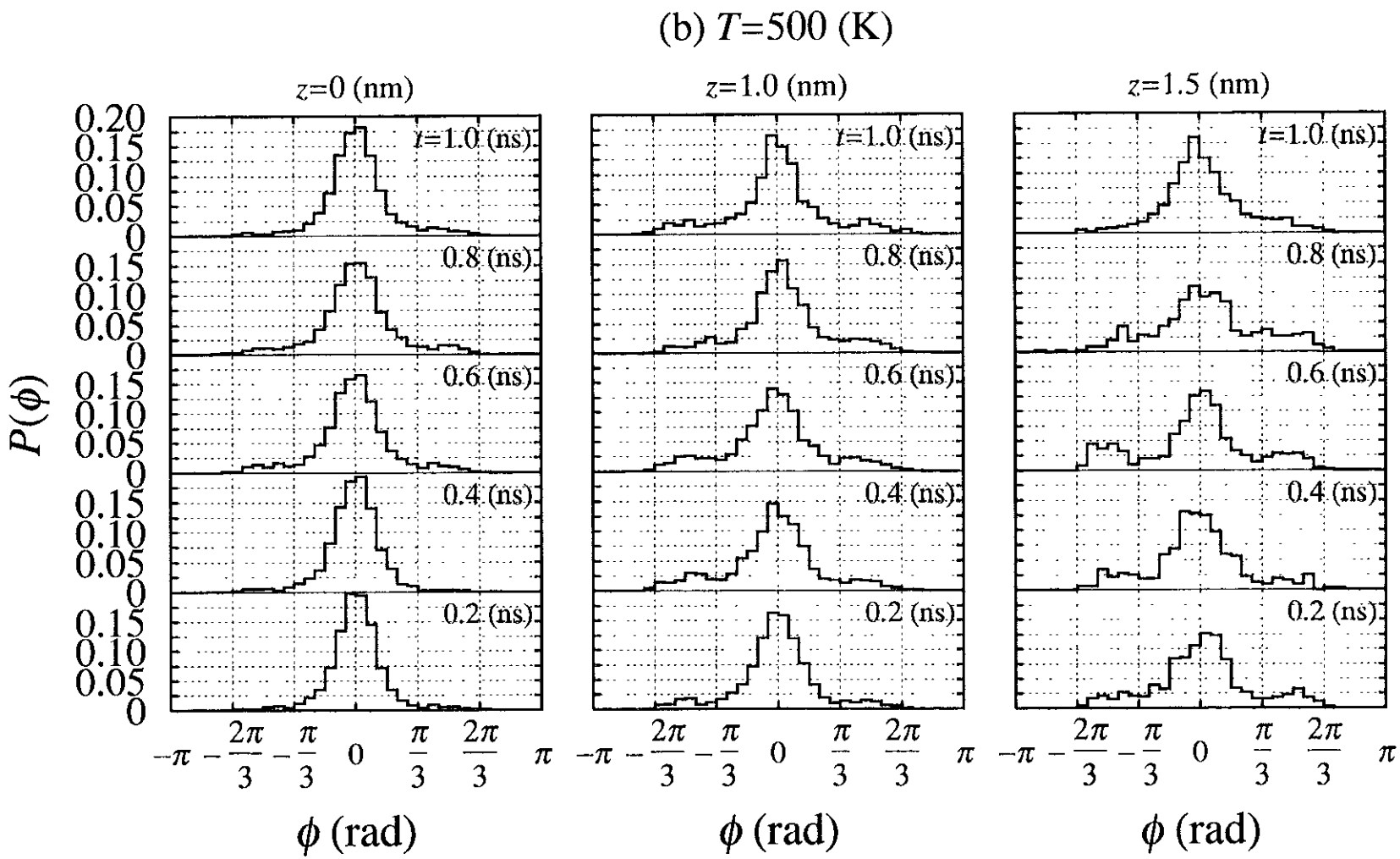
(b) T=500 (K)
z=0 (nm)
z=1.0 (nm)
z=1.5 (nm)
t=1.0 (ns)
0.8 (ns)
0.6 (ns)
0.4 (ns)
0.2 (ns)
$P(\phi)$
0.20
0.15
0.10
0.05
0
$-\pi$ $-\frac{2\pi}{3}$ $-\frac{\pi}{3}$ 0 $\frac{\pi}{3}$ $\frac{2\pi}{3}$ π
ϕ (rad)

Fig. 13(b)

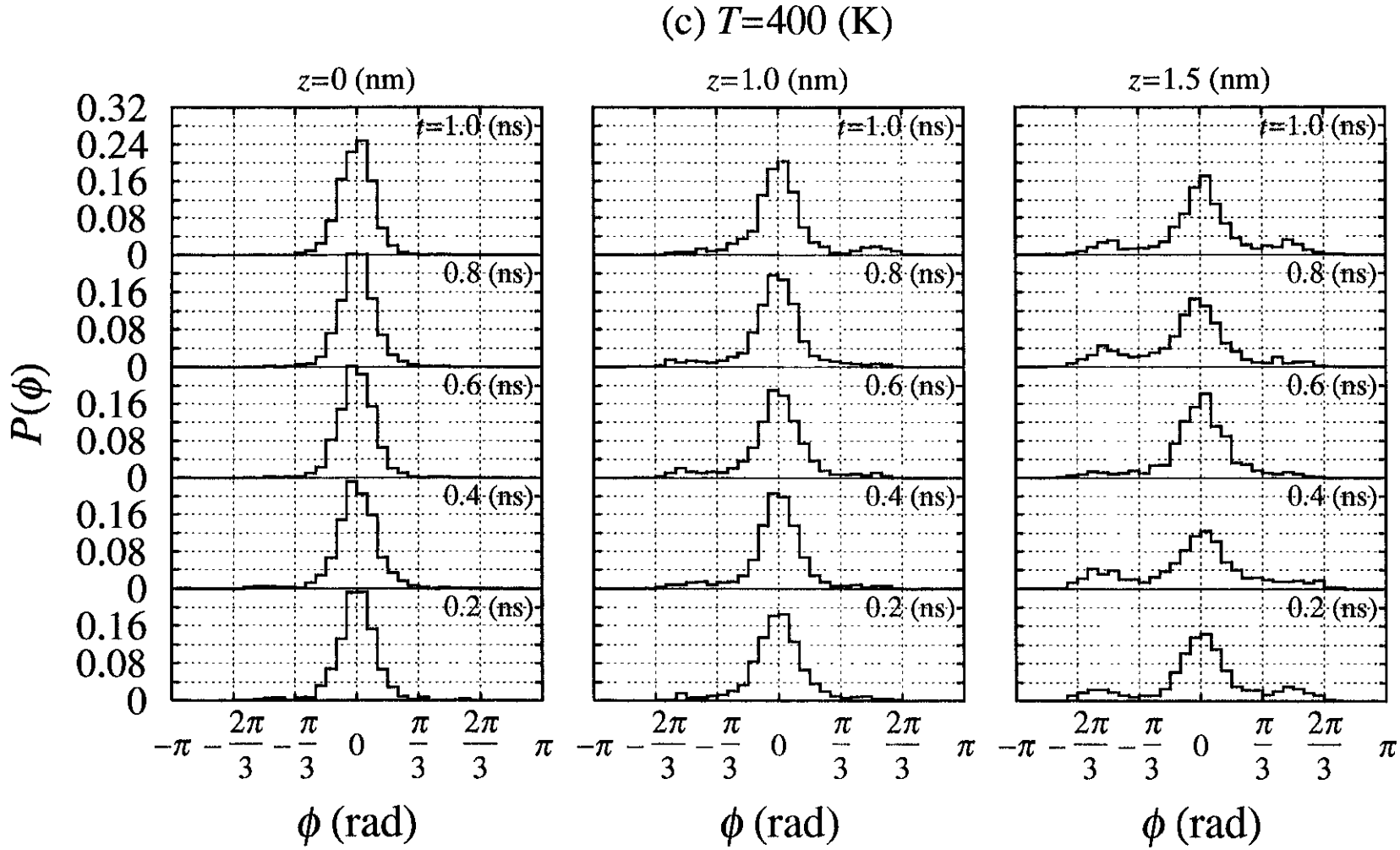
(c) T=400 (K)
z=0 (nm)
z=1.0 (nm)
z=1.5 (nm)
t=1.0 (ns)
0.8 (ns)
0.6 (ns)
0.4 (ns)
0.2 (ns)
$P(\phi)$
0.32
0.24
0.16
0.08
0
$-\pi$ $-\frac{2\pi}{3}$ $-\frac{\pi}{3}$ 0 $\frac{\pi}{3}$ $\frac{2\pi}{3}$ π
ϕ (rad)

Fig. 13(c)

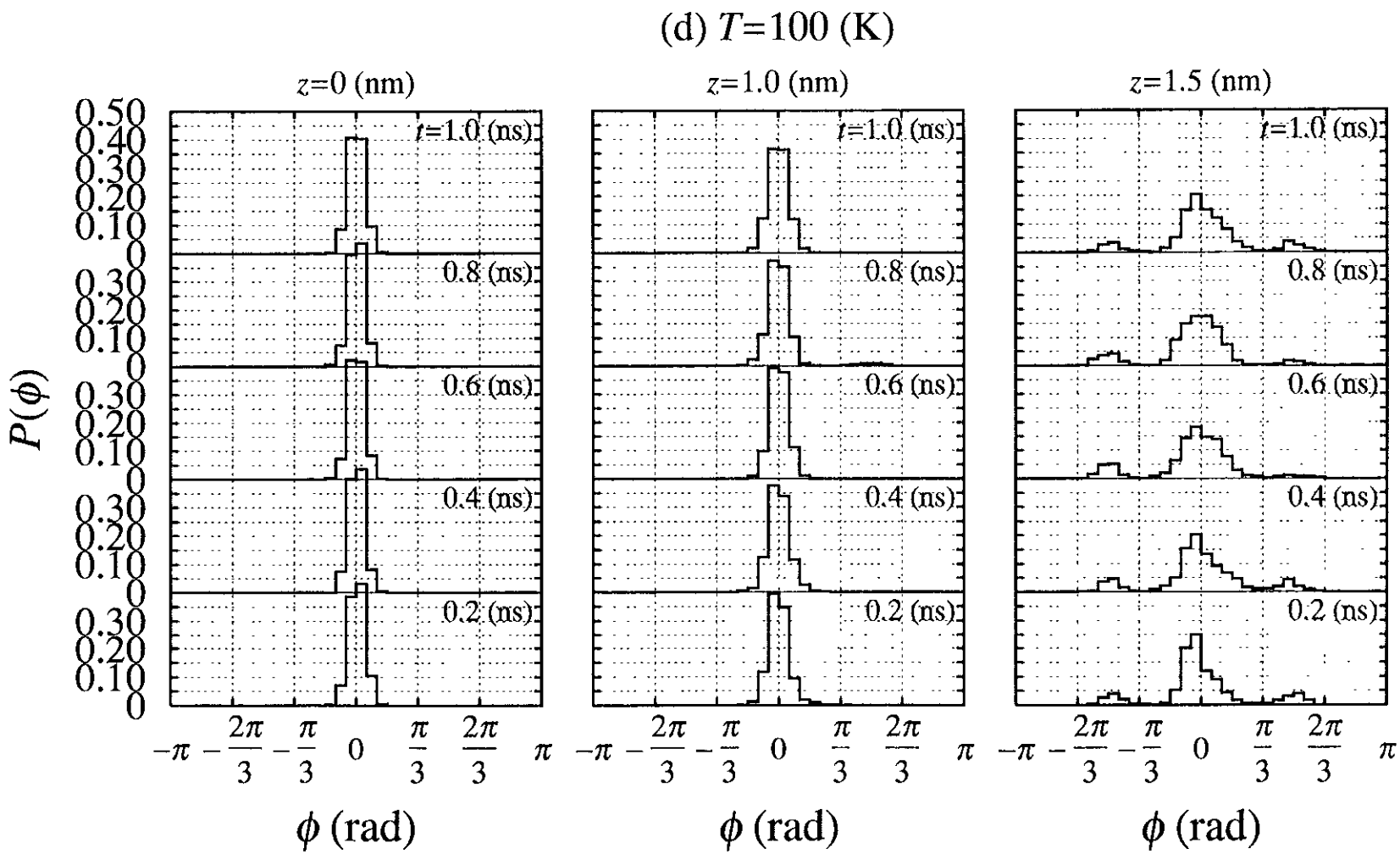
(d) T=100 (K)
z=0 (nm)
z=1.0 (nm)
z=1.5 (nm)
t=1.0 (ns)
0.8 (ns)
0.6 (ns)
0.4 (ns)
0.2 (ns)
$P(\phi)$
0.50
0.40
0.30
0.20
0.10
0
$-\pi$ $-\frac{2\pi}{3}$ $-\frac{\pi}{3}$ 0 $\frac{\pi}{3}$ $\frac{2\pi}{3}$ π
ϕ (rad)

Fig. 13(d)

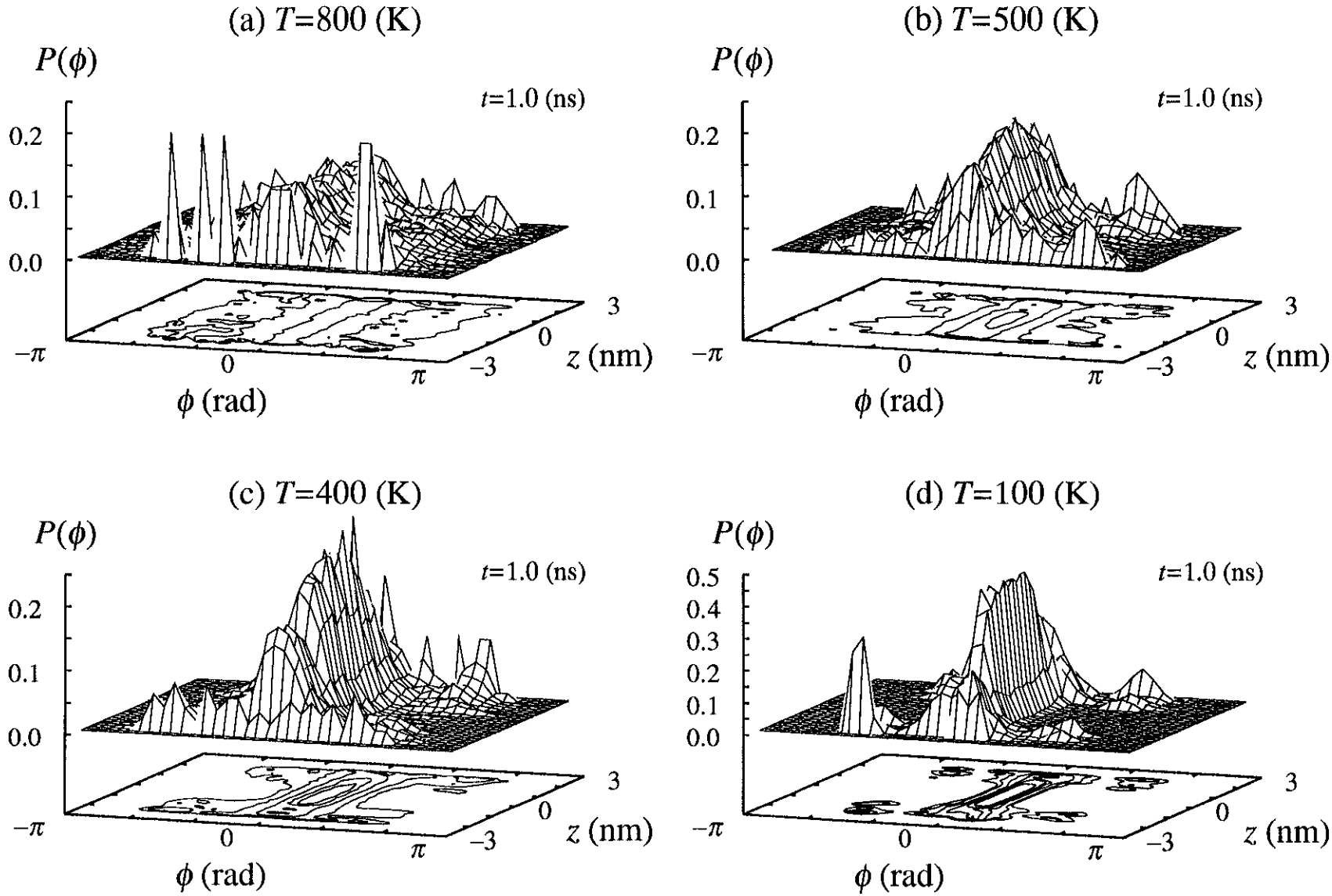
(a) T=800 (K)
P(φ)
t=1.0 (ns)
0.2
0.1
0.0
−π
0
π
φ (rad)
3
0
−3
z (nm)
(b) T=500 (K)
P(φ)
t=1.0 (ns)
0.2
0.1
0.0
−π
0
π
φ (rad)
3
0
−3
z (nm)
(c) T=400 (K)
P(φ)
t=1.0 (ns)
0.2
0.1
0.0
−π
0
π
φ (rad)
3
0
−3
z (nm)
(d) T=100 (K)
P(φ)
t=1.0 (ns)
0.5
0.4
0.3
0.2
0.1
0.0
−π
0
π
φ (rad)
3
0
−3
z (nm)

Fig. 14

Recent Issues of NIFS Series

NIFS-441 O. Kaneko, Y. Takeiri, K. Tsumori, Y. Oka, M. Osakabe, R. Akiyama, T. Kawamoto, E. Asano and T. Kuroda,
Development of Negative-Ion-Based Neutral Beam Injector for the Large Helical Device; Sep. 1996 (IAEA-CN-64/GP-9)

NIFS-442 K. Toi, K.N. Sato, Y. Hamada, S. Ohdachi, H. Sakakita, A. Nishizawa, A. Ejiri, K. Narihara, H. Kuramoto, Y. Kawasumi, S. Kubo, T. Seki, K. Kitachi, J. Xu, K. Ida, K. Kawahata, I. Nomura, K. Adachi, R. Akiyama, A. Fujisawa, J. Fujita, N. Hiraki, S. Hidekuma, S. Hirokura, H. Idei, T. Ido, H. Iguchi, K. Iwasaki, M. Isobe, O. Kaneko, Y. Kano, M. Kojima, J. Koog, R. Kumazawa, T. Kuroda, J. Li, R. Liang, T. Minami, S. Morita, K. Ohkubo, Y. Oka, S. Okajima, M. Osakabe, Y. Sakawa, M. Sasao, K. Sato, T. Shimpo, T. Shoji, H. Sugai, T. Watari, I. Yamada and K. Yamauti,
Studies of Perturbative Plasma Transport, Ice Pellet Ablation and Sawtooth Phenomena in the JIPP T-IIU Tokamak; Sep. 1996 (IAEA-CN-64/A6-5)

NIFS-443 Y. Todo, T. Sato and The Complexity Simulation Group,
Vlasov-MHD and Particle-MHD Simulations of the Toroidal Alfvén Eigenmode; Sep. 1996 (IAEA-CN-64/D2-3)

NIFS-444 A. Fujisawa, S. Kubo, H. Iguchi, H. Idei, T. Minami, H. Sanuki, K. Itoh, S. Okamura, K. Matsuoka, K. Tanaka, S. Lee, M. Kojima, T.P. Crowley, Y. Hamada, M. Iwase, H. Nagasaki, H. Suzuki, N. Inoue, R. Akiyama, M. Osakabe, S. Morita, C. Takahashi, S. Muto, A. Ejiri, K. Ida, S. Nishimura, K. Narihara, I. Yamada, K. Toi, S. Ohdachi, T. Ozaki, A. Komori, K. Nishimura, S. Hidekuma, K. Ohkubo, D.A. Rasmussen, J.B. Wilgen, M. Murakami, T. Watari and M. Fujiwara,
An Experimental Study of Plasma Confinement and Heating Efficiency through the Potential Profile Measurements with a Heavy Ion Beam Probe in the Compact Helical System; Sep. 1996 (IAEA-CN-64/C1-5)

NIFS-445 O. Motojima, N. Yanagi, S. Imagawa, K. Takahata, S. Yamada, A. Iwamoto, H. Chikaraishi, S. Kitagawa, R. Maekawa, S. Masuzaki, T. Mito, T. Morisaki, A. Nishimura, S. Sakakibara, S. Satoh, T. Satow, H. Tamura, S. Tanahashi, K. Watanabe, S. Yamaguchi, J. Yamamoto, M.Fujiwara and A. Iiyoshi,
Superconducting Magnet Design and Construction of LHD; Sep. 1996 (IAEA-CN-64/G2-4)

NIFS-446 S. Murakami, N. Nakajima, S. Okamura, M. Okamoto and U. Gasparino,
Orbit Effects of Energetic Particles on the Reachable β–Value and the Radial Electric Field in NBI and ECR Heated Heliotron Plasmas; Sep. 1996 (IAEA-CN-64/CP -6) Sep. 1996

NIFS-447 K. Yamazaki, A. Sagara, O. Motojima, M. Fujiwara, T. Amano, H. Chikaraishi, S. Imagawa, T. Muroga, N. Noda, N. Ohyabu, T. Satow, J.F. Wang, K.Y. Watanabe, J. Yamamoto . H. Yamanishi, A. Kohyama, H. Matsui, O. Mitarai, T. Noda, A.A. Shishkin, S. Tanaka and T. Terai
Design Assessment of Heliotron Reactor; Sep. 1996 (IAEA-CN-64/G1-5)

NIFS-448 M. Ozaki, T. Sato and the Complexity Simulation Group,
Interactions of Convecting Magnetic Loops and Arcades; Sep. 1996

NIFS-449 T. Aoki,
Interpolated Differential Operator (IDO) Scheme for Solving Partial Differential Equations; Sep. 1996

NIFS-450 D. Biskamp and T. Sato,
Partial Reconnection in the Sawtooth Collapse; Sep. 1996

NIFS-451 J. Li, X. Gong, L. Luo, F.X. Yin, N. Noda, B. Wan, W. Xu, X. Gao, F. Yin, J.G. Jiang, Z. Wu., J.Y. Zhao, M. Wu, S. Liu and Y. Han,
Effects of High Z Probe on Plasma Behavior in HT-6M Tokamak; Sep. 1996

NIFS-452 N. Nakajima, K. Ichiguchi, M. Okamoto and R.L. Dewar,
Ballooning Modes in Heliotrons/Torsatrons; Sep. 1996 (IAEA-CN-64/D3-6)

NIFS-453 A. Iiyoshi,
Overview of Helical Systems; Sep. 1996 (IAEA-CN-64/O1-7)

NIFS-454 S. Saito, Y. Nomura, K. Hirose and Y.H. Ichikawa,
Separatrix Reconnection and Periodic Orbit Annihilation in the Harper Map; Oct. 1996

NIFS-455 K. Ichiguchi, N. Nakajima and M. Okamoto,
Topics on MHD Equilibrium and Stability in Heliotron / Torsatron; Oct. 1996

NIFS-456 G. Kawahara, S. Kida, M. Tanaka and S. Yanase,
Wrap, Tilt and Stretch of Vorticity Lines around a Strong Straight Vortex Tube in a Simple Shear Flow; Oct. 1996

NIFS-457 K. Itoh, S.- I. Itoh, A. Fukuyama and M. Yagi,
Turbulent Transport and Structural Transition in Confined Plasmas; Oct. 1996

NIFS-458 A. Kageyama and T. Sato,
Generation Mechanism of a Dipole Field by a Magnetohydrodynamic Dynamo; Oct. 1996

NIFS-459 K. Araki, J. Mizushima and S. Yanase,
The Non-axisymmetric Instability of the Wide-Gap Spherical Couette Flow; Oct. 1996

NIFS-460 Y. Hamada, A. Fujisawa, H. Iguchi, A. Nishizawa and Y. Kawasumi,
A Tandem Parallel Plate Analyzer; Nov. 1996

NIFS-461 Y. Hamada, A. Nishizawa, Y. Kawasumi, A. Fujisawa, K. Narihara, K. Ida, A. Ejiri, S. Ohdachi, K. Kawahata, K. Toi, K. Sato, T. Seki, H. Iguchi, K. Adachi, S. Hidekuma,

S.Hirokura, K. Iwasaki, T. Ido, M. Kojima, J. Koong, R. Kumazawa, H. Kuramoto, T. Minami, I. Nomura, H Sakakita, M. Sasao, K.N. Sato, T. Tsuzuki, J. Xu, I. Yamada and T. Watari,
Density Fluctuation in JIPP T-IIU Tokamak Plasmas Measured by a Heavy Ion Beam Probe; Nov. 1996

NIFS-462 N. Katsuragawa, H. Hojo and A. Mase,
Simulation Study on Cross Polarization Scattering of Ultrashort-Pulse Electromagnetic Waves; Nov. 1996

NIFS-463 V. Voitsenya, V. Konovalov, O. Motojima, K. Narihara, M. Becker and B. Schunke,
Evaluations of Different Metals for Manufacturing Mirrors of Thomson Scattering System for the LHD Divertor Plasma; Nov. 1996

NIFS-464 M. Pereyaslavets, M. Sato, T. Shimozuma, Y. Takita, H. Idei, S. Kubo, K. Ohkubo and K. Hayashi,
Development and Simulation of RF Components for High Power Millimeter Wave Gyrotrons; Nov. 1996

NIFS-465 V.S. Voitsenya, S. Masuzaki, O. Motojima, N. Noda and N. Ohyabu,
On the Use of CX Atom Analyzer for Study Characteristics of Ion Component in a LHD Divertor Plasma; Dec. 1996

NIFS-466 H. Miura and S. Kida,
Identification of Tubular Vortices in Complex Flows; Dec. 1996

NIFS-467 Y. Takeiri, Y. Oka, M. Osakabe, K. Tsumori, O. Kaneko, T. Takanashi, E. Asano, T. Kawamoto, R. Akiyama and T. Kuroda,
Suppression of Accelerated Electrons in a High-current Large Negative Ion Source; Dec. 1996

NIFS-468 A. Sagara, Y. Hasegawa, K. Tsuzuki, N. Inoue, H. Suzuki, T. Morisaki, N. Noda, O. Motojima, S. Okamura, K. Matsuoka, R. Akiyama, K. Ida, H. Idei, K. Iwasaki, S. Kubo, T. Minami, S. Morita, K. Narihara, T. Ozaki, K. Sato, C. Takahashi, K. Tanaka, K. Toi and I. Yamada,
Real Time Boronization Experiments in CHS and Scaling for LHD; Dec. 1996

NIFS-469 V.L. Vdovin, T.Watari and A. Fukuyama,
3D Maxwell-Vlasov Boundary Value Problem Solution in Stellarator Geometry in Ion Cyclotron Frequency Range (final report); Dec. 1996

NIFS-470 N. Nakajima, M. Yokoyama, M. Okamoto and J. Nührenberg,
Optimization of M=2 Stellarator; Dec. 1996

NIFS-471 A. Fujisawa, H. Iguchi, S. Lee and Y. Hamada,
Effects of Horizontal Injection Angle Displacements on Energy Measurements with Parallel Plate Energy Analyzer; Dec. 1996

NIFS-472 R. Kanno, N. Nakajima, H. Sugama, M. Okamoto and Y. Ogawa,

Effects of Finite-β and Radial Electric Fields on Neoclassical Transport in the Large Helical Device; Jan. 1997

NIFS-473 S. Murakami, N. Nakajima, U. Gasparino and M. Okamoto,
Simulation Study of Radial Electric Field in CHS and LHD; Jan. 1997

NIFS-474 K. Ohkubo, S. Kubo, H. Idei, M. Sato, T. Shimozuma and Y. Takita,
Coupling of Tilting Gaussian Beam with Hybrid Mode in the Corrugated Waveguide; Jan. 1997

NIFS-475 A. Fujisawa, H. Iguchi, S. Lee and Y. Hamada,
Consideration of Fluctuation in Secondary Beam Intensity of Heavy Ion Beam Prove Measurements; Jan. 1997

NIFS-476 Y. Takeiri, M. Osakabe, Y. Oka, K. Tsumori, O. Kaneko, T. Takanashi, E. Asano, T. Kawamoto, R. Akiyama and T. Kuroda,
Long-pulse Operation of a Cesium-Seeded High-Current Large Negative Ion Source; Jan. 1997

NIFS-477 H. Kuramoto, K. Toi, N. Haraki, K. Sato, J. Xu, A. Ejiri, K. Narihara, T. Seki, S. Ohdachi, K. Adati. R. Akiyama, Y. Hamada, S. Hirokura, K. Kawahata and M. Kojima,
Study of Toroidal Current Penetration during Current Ramp in JIPP T-IIU with Fast Response Zeeman Polarimeter; Jan. 7, 1997

NIFS-478 H. Sugama and W. Horton,
Neoclassical Electron and Ion Transport in Toroidally Rotating Plasmas; Jan. 1997

NIFS-479 V.L. Vdovin and I.V. Kamenskij,
3D Electromagnetic Theory of ICRF Multi Port Multi Loop Antenna; Jan. 1997

NIFS-480 W.X. Wang, M. Okamoto, N. Nakajima, S Murakami and N. Ohyabu,
Cooling Effect of Secondary Electrons in the High Temperature Divertor Operation; Feb. 1997

NIFS-481 K. Itoh, S.-I. Itoh, H. Soltwisch and H.R. Koslowski,
Generation of Toroidal Current Sheet at Sawtooth Crash; Feb. 1997

NIFS-482 K. Ichiguchi,
Collisionality Dependence of Mercier Stability in LHD Equilibria with Bootstrap Currents; Feb. 1997

NIFS-483 S. Fujiwara and T. Sato,
Molecular Dynamics Simulations of Structural Formation of a Single Polymer Chain: Bond-orientational Order and Conformational Defects; Feb. 1997